2012

Examination of Spatial Variations in Recrystallization Mechanisms in Quartz

Emma N. Beck
Colby College

EXAMINATION OF SPATIAL VARIATIONS IN RECRYSTALLIZATION MECHANISMS IN QUARTZ

Emma N. Beck ‘12

A Thesis

Submitted to the Faculty of the Geology Department
of Colby College in Fulfillment of the Requirements for
Honors in Geology

Waterville, ME
May 2012

EXAMINATION OF SPATIAL VARIATIONS IN RECRYSTALLIZATION MECHANISMS IN QUARTZ

Except where reference is made to the work of others, the work described in this thesis is my own or was done in collaboration with my advisory committee

Emma N. Beck '12

Certificate of Approval:

Dr. Walter A. Sullivan
Assistant Professor
Department of Geology

Dr. Rachel J. Beane
Professor, Bowdoin College
Department of Earth and
Oceanographic Sciences

Dr. Robert A. Gastaldo
Whipple Coddington Professor
Department of Geology

Abstract

S-C mylonites form as a result of non-coaxial deformation in ductile shear zones. Planes of weakness develop and delineate two domains, the S and the C Each of these domains accommodates variable amounts of strain. Sample WMSZ-188 exhibits subgrain rotation (SGR) recrystallization in the C domains, and grain boundary migration (GBM) recrystallization in the S domains. This partitioning of recrystallization mechanisms indicates either: (1) strain-rate partitioning during a single deformation event; or (2) a second, lower-temperature deformation event that over-printed the C domains. This study tests these two hypotheses. Optical and EBSD analyses were used to look for evidence of a second phase of lower-temperature deformation in the S domains. The quartz grains in the S domains exhibit some areas of internal misorientation, however these zones are not interpreted as being a result of a SGR recrystallization overprint. High-temperature microstructures in feldspar and biotite also are preserved throughout the sample, indicating that no late-stage, low-temperature deformation over-printing occurred. These observations, in conjunction with optical analyses of samples from the region, indicate that these two recrystallization mechanisms are coeval. Because the sample does not record a syndeformational decrease in temperature and probably records nearly isobaric deformation due to its setting in a strike-slip fault system, the simultaneous generation of the recrystallization mechanisms is attributed to domainal strain-rate partitioning during a single deformation event. One to three orders of magnitude of difference in strain-rate is required to transition from one recrystallization mechanism to another between the S and C domains. The implication of this domainal strain-rate partitioning is that caution must be exercised when using recrystallization mechanisms to determine deformation temperature.

Acknowledgements

Many, many thanks to Dr. Walter “Bill” Sullivan for answering all of my never-ending questions and for giving me the confidence I needed to get through my thesis. I never would have thought that this was his first advising of an honors thesis. Thanks to Dr. Rachel Beane for fighting for me, against man and machine, to ensure that I got my project back on course. Her insight and suggestions helped enhance my understanding of concepts and ultimately the quality of my thesis. Thanks also to Dr. Robert Gastaldo for his astute edits and comments, as well as his help along the way. Last, but not least, a big thanks to my friends and family for putting up with my frequent disappearances into Mudd and for their support of my research, even if they never understood any of it.

Table of Contents

1. Introduction

Mylonites are dynamically recrystallized metamorphic rocks formed in a zone of non-coaxial deformation (Snoke et al., 1998). Shear zones, such as those in which mylonites form, are very common around the world; some include the Pernambuco shear zone in Brazil, Norumbega shear zone in eastern Maine, Tonale fault zone in the southern Alps, and the central African shear zone (Stipp et al., 2002; Wang and Ludman, 2004; Nzenti et al., 2006; Lopes et al., 2009). These shear zones accommodated a large amount of deformation in the past. Deformation fabrics that form in mylonites in these shear zones frequently are used as sense of shear indicators and paleo-thermometers (Stipp et al., 2002; Sullivan and Law, 2007).

As a result of the simple shear strain and subsequent crystal-plastic flow, mylonites commonly form two different foliations, S and C, and have strong crystallographic preferred orientations (CPOs) (Lister and Snoke, 1984). The C foliations in these rocks accommodate the majority of the strain, while the S foliations form as a result of relatively minor amounts of strain (Lister and Snoke, 1984). These create different domains within the mylonites: the S and C domains. Fabrics of S-C mylonites have been used as shear sense indicators in high-strain rocks from around the world (e.g. Jain and Manickavasagam, 1993; Corsini et al., 1995; Wang and Ludman, 2004; Sullivan and Law, 2007; Biswal et al., 2010).

Quartz in mylonites responds to deformation by dynamically recrystallizing, and the recrystallization mechanisms commonly are used to

estimate deformation temperature. There are three primary mechanisms by which quartz grains recrystallize: grain boundary migration (GBM), subgrain rotation (SGR), and bulging (BLG). These mechanisms are controlled by temperature, strain rate, and water fugacity. GBM occurs in the highest temperature and/or lowest strain rate environments (Hirth and Tullis, 1992; Stipp et al., 2002). During GBM recrystallization, the high temperatures allow the grains with low internal strain energy to consume other grains with high internal strain energy (Hirth and Tullis, 1992; Stipp et al., 2002). In contrast, SGR occurs under lower temperature and/or higher strain rate conditions. During SGR recrystallization, dislocations gradually concentrate at subgrain boundaries and eventually accumulate to a point where the crystal lattice bends enough to create a new grain (Hirth and Tullis, 1992). BLG occurs at the lowest temperatures and/or highest strain rates when grain boundaries migrate at the 10-μm scale to form lobate, sutured boundaries and very small neoblasts (Hirth and Tullis, 1992). This process also is driven by dislocation density, but the low temperatures do not allow for significant grain-boundary migration (Paschier and Trouw, 2005). These recrystallization mechanisms are not confined to isolated conditions but, instead, there are continuous changes in the rates of grain-boundary migration and subgrain rotation (Fig. 1, Stipp et al., 2002, 2010). The transition between these regimes is gradual (Tullis, 1992).

Sullivan and Law (2007) discovered an S-C mylonite that exhibits GBM recrystallization in the S domains and SGR recrystallization in the C domains (Fig. 2). Two hypotheses can explain this phenomenon: (1) either there was one

deformational event during which both of the recrystallization mechanisms operated, or (2) the quartz deformed during two deformational events . If the first hypothesis is correct, there should be significant overprinting of SGR recrystallization atop the grains that exhibit predominantly GBM recrystallization. If two deformation phases are recorded, GBM recrystallization must have occurred first because a late phase of relatively high-temperature GBM recrystallization should recrystallize the entire sample. Late-phase, relatively low-temperature deformation could easily be localized, however.

If the second hypothesis is correct, predominantly GBM recrystallization should be recorded in the S foliation. This would indicate that strain-rate partitioning is responsible for the different recrystallization mechanisms. When these differing recrystallization mechanisms are operating within millimeters of one another during a single deformation event, neither water fugacity nor temperature variation can be responsible for the discordance. In such a case, the C foliation accommodates the majority of the strain while the S foliation absorbs a smaller amount of strain. To test these two hypotheses, this study focuses on the recrystallized quartz textures and crystallographic orientations as constraints on the recrystallization mechanisms that operated in the S and C domains. The results of this study provide a better understanding of how S-C mylonites form by constraining the magnitude of this potential strain-rate partitioning between the S and C domains.

2. Geologic Setting

2.1 *Regional Geology*

The White Mountain shear zone (WMSZ) is a Late Cretaceous dextral transpressional fault system located in the White Mountains in eastern California and western Nevada. In the study area the shear zone primarily cuts two plutons, the 90-Ma Pellisier Flats pluton, a biotite hornblende granite/quartz monzonite, and the younger Boundary Peak pluton, a biotite granite (McKee and Conrad, 1996) (Fig. 3). Where it is cute by the WMSZ, the Pellisier Flats pluton is highly deformed with a strong, solid-state deformation fabric. It hosts almost the entire Boundary Peak pluton as well as local quartz-rich skarns (xenoliths) (Crowder et al., 1972). The Boundary Peak pluton likely intruded during deformation because it exhibits a weak solid-state fabric at its margins (Sullivan and Law, 2007). This indicates that deformation along the WMSZ was near completion when the Boundary Peak pluton crystallized (Crowder et al., 1972). Deformation in the WMSZ must have continued for a time after the crystallization of the Boundary Peak pluton because the deformed quartz in the Pellisier Flats pluton within 400 m of the margins of the Boundary Peak pluton did not undergo static annealing recrystallization (Sullivan and Law, 2007). Deformation must have ceased by 73 Ma when the biotite cooling ages were reached in the Boundary Peak pluton (Crowder et al, 1973, McKee and Conrad, 1996, Sullivan, 2003 [M.S. Thesis]).

2.2 Sample Descriptions

2.2.1 *Sample WMSZ-188 Description*

Sample WMSZ-188 is an S-C mylonite from the White Mountain shear zone. It was derived from the Pellisier Flats pluton (Sullivan and Law, 2007) and was collected ~700 m from the Boundary Peak pluton (Fig. 3). It contains biotite, potassium feldspar, plagioclase feldspar, quartz, and various opaque minerals. Based on visual estimates, there is a quartz content of ~50%. Flattened and elongated minerals create subvertical foliations and subhorizontal lineations on C surfaces resulting from dextral simple shearing (Sullivan and Law, 2007). This sample exhibits differing recrystallization mechanisms within the S and C domains (Sullivan and Law, 2007). The microstructural fabric of WMSZ-188, as described by Sullivan and Law (2007), is characteristic of GBM and SGR recrystallization in the S and C domains respectively. Quartz *c*-axis fabrics collected from C domains have maxima that indicate slip on the rhomb system while *c*-axis fabrics collected from both the C and S domains have maxima indicative of slip on the prism system (Sullivan and Law, 2007). Because slip on the rhomb system occurs at a lower temperature and/or at higher strain rates relative to slip on the prism system, these data also indicate that strain partitioning may have occurred between the two domains (Schmid and Casey, 1986).

2.2.2 *Samples WMSZ-103, 065, and 069*

Sample WMSZ-103 is an S-C mylonite that was collected from the deformed Pellisier Flats pluton in a transect 1.6–1.7 km to the south of WMSZ-

188 (Fig. 3). This biotite, hornblende granite was collected ~200 m from the Boundary Peak pluton. Sample WMSZ-103 has a lower quartz content than sample WMSZ-188 (~25% based on visual estimations).

Samples WMSZ-065 and -069 were collected ~6.4 km south of WMSZ-188 along Mongomery Canyon ~200 m from an exposure of the Boundary Peak pluton (Fig. 3). They are deformed metasedimentary rocks that are ~ 90% quartz (based on visual estimates). The samples also contain calcite, clinopyroxene, garnet, zoesite, opaque phases and retrograde chlorite (Sullivan and Law, 2007).

3. Methods

3.1 Introduction

There are a variety of ways to determine recrystallization mechanisms in deformed rocks. To test the two-deformational-phase hypothesis, I determined if significant subgrain formation occurred within the grains that exhibit characteristics typical of GBM recrystallization. Even if the possible second low-temperature event did not have a significant enough impact on the S domains to completely recrystallize them via SGR recrystallization, it is likely that some evidence of SGR recrystallization would exist in the internal misorientations of the quartz crystal lattices (Piazolo et al., 2005).

Microstructural observations were made using a petrographic microscope. The quartz microstructural properties were characterized using cross-polarized light with and without the gypsum plate. Other structures were noted, particularly those indicative of low-temperature deformation over-printing. These include biotite-chlorite replacement and dynamic recrystallization of minerals other than

quartz (i.e. feldspar). Samples from other areas in the WMSZ contain correlative structures that help interpret WMSZ-188 also were characterized visually. Thin sections are cut perpendicular to foliation and parallel with the stretching lineation on the C surfaces (note, all photomicrographs and EBSD maps have an apparent sinistral sense because of the way the thin section was cut).

To detect any recrystallization overprinting in the quartz, the crystallographic orientation was mapped within and between grains in both the S and C domains using SEM Electron-backscatter-diffraction patterns (EBSD). This EBSD mapping illustrates whether there is any evidence of significant subgrain formation in the S domains. The EBSD data were also used to determine the dominant slip systems in the C domains. Further description of the ESBD methods is available in Appendix A.

Many methods of identifying subgrains have been reported in the literature. For example, Simpson (1998) defines a subgrain simply as visibly distinct misorientations that are observable in cross-polarized light but not in plane polarized light. Other authors, such as Pachier and Touw (2005), define a subgrain as a dislocation-induced boundary that separates two volumes of a crystal with the same composition that have rotated less than 5° with respect to each other. This study employs both of these techniques to identify subgrain formation. Optical analyses use Simpson's (1998) definition, however accurately detecting slight offset requires crystallographic mapping at sub-mm intervals; thus, EBSD analyses use Paschier and Trouw's (2005) definition. For the purpose of this study, subgrains are considered zones of internal misorientation

within a grain and high-angle grain boundaries are defined as misorientation > 20° across grain boundaries.

3.2 EBSD Data Collection

EBSD data were collected from two areas on sample WMSZ-188, site 1 and site 2 (Fig. 4). These sites were chosen because they contain dynamically recrystallized quartz grains that exhibit SGR- and GBM-like features adjacent to each other, and they are large enough and contain enough grains for meaningful analyses. The data were collected with a SEM at Bowdoin College equipped with a HKL Nordlys II detector and Channel 5 software (software details in Schmidt and Olesen, 1989). Samples were prepared by chemically polishing microprobe quality thin sections approximately four to five hours in a non-crystallizing colloidal silica suspension on a vibratory polisher (SYTON method of Fynn and Powell, 1979). Thin sections were not carbon coated; charging was minimized by using a chamber pressure of 15 Pa, combined with the 70° tilt required for pattern acquisition. Operating parameters include an accelerating voltage of 20 kV, a working distance of 25 mm, and a beam current of 2.2 nA. EBSD sampling techniques are based on those used by Sullivan and Beane (2010). Channel 5 acquisition and indexing settings were 4x4 binning, high gain, 6 frames averaged, Hough resolution = 65, 6 bands, and 85 reflectors. Quartz was indexed using the lattice parameters of Sands (1969). Accepted data points were limited to those with mean angular deviations (MAD) less than 1.5° based on the number of bands (6) detected compared to the experimental work of Krieger Lassen (1996) on the precision of crystal orientations. MAD is the degree of

angular misfit of the simulated image from the actual image. EBSD patterns were collected in an automated mapping mode with a 2-μm step size that should have allowed collection of at least 6 data points per grain if all data points were indexed correctly. Grains indexed with less than 6 points per grain were not used for analyses.

Grains were grown to completion using an iterative extrapolation routine in which non-indexed data points acquired the average orientation of 6 neighbors. Prior et al. (2009) demonstrated that this method does not create substantial artifacts. The extrapolation process infers the orientation for zero-solution points based on a give number of neighbor points (6 in this study); this could potentially create artifacts that would skew the data by creating false grains or changing the data points' orientations. Zero-solution points are data points that were not indexed; this can be due to a variety of reasons, such as an imperfection, poor focus, or a MAD that exceeds the threshold parameters.

Two analytical techniques were used to process the data: texture-component maps and misorientation profiles. Texture-component maps illustrate misorientation within an individual grain with regards to the orientation of a chosen point. The maps in this study are relative to a centered point in the grain. The 2-D misorientation profiles are based on a transect line that can be drawn anywhere on the map. These profiles are displayed relative to the first point at one end of the profile. They were created before the extrapolation of the grains was performed to ensure the data was not altered.

4. Results

4.1 *Optical analyses*

4.1.1 *Sample WMSZ-188*

The S domains in sample WMSZ-188 contain elongated, lobate, and amoeboid quartz crystals along with island grains; all of these features are typical of GBM recrystallization. The C domains in this sample contain small, elongated quartz grains with gradational, indistinct grain boundaries characteristic of SGR recrystallization, and many well-developed subgrains (Fig. 5). In one area of the thin section a single ribbon of quartz extends from one C domain, completely through the S domain, to another C domain (Fig. 2). Where this ribbon lies in the C domains, quartz is dominated by SGR recrystallization, and where it lies in the S domain, quartz is dominated by GBM recrystallization.

Plastically deformed and dynamically recrystallized feldspars are visible throughout the sample but were not mapped using EBSD. Round, fine-grained (2-10 μm) feldspar crystals with serrated boundaries adjacent to the old grains are found throughout the sample but are generally concentrated along the C foliations (Fig. 6a). These grains record BLG recrystallization. The relict feldspar grains between the S foliation surfaces also exhibit sweeping, undulose extinction and subgrain formation (Fig. 6b). There is also extensive myrmekite growth in the feldspars throughout the sample (Fig. 6b). Biotite crystals are locally layered with the recrystallized feldspars in the C domains and are aligned parallel to the C foliation. Biotite in WMSZ-188 is not altered to chlorite.

4.1.2 *Samples WMSZ-065 and -069*

The dynamically recrystallized quartz grains in samples WMSZ-065 and -069 are relatively large, lobate, and amoeboid in shape and they exhibit grain consumption; all of these features are typical of GBM recrystallization (Figs. 7, 8). In WMSZ-065 and -069, some island grains that are contiguous with their parent grains exhibit sweeping undulose extinction (Figs. 7, 8). These island grains are partially consumed by almost entirely strain-free quartz grains. Therefore, the internal misorientation in the island grains resulting in the sweeping undulose extinction must predate or be coeval with the GBM recrystallization. The island grains depicted in Figure 8 go entirely extinct over a stage rotation of ~20°. This is a good minimum estimate for the amount of internal misorientation in these grains. The middle of the grain c (Fig. 7, 8) goes extinct first with wavy extinction patterns moving out from the center. The island grains also exhibit gradational grain boundaries that alter the apparent grain shape as the sweeping extinction moves across the grains (Fig. 8). The grains' amoeboid arm-like extensions have small areas within them that go extinct at different orientations and exhibit subgrain-like qualities (Fig. 8). Other grains in this sample exhibit similar changes in the appearance of their grain boundaries and internal misorientation (Fig. 8).

4.1.3 *Sample WMSZ-103*

Sample WMSZ-103 contains small, elongate quartz grains with blurry grain boundaries in C domains that transition into the larger grains in the S domains with more distinct grain boundaries. This microstructure is very similar

SGR and SGR-GBM transitional zone seen in WMSZ-188. The quartz grains in this sample are predominantly recrystallized via SGR with some areas that record a transition between SGR and GBM recrystallization (Fig. 10). The recrystallized quartz in WMSZ-103 is frequently pinched between feldspar grains. Dynamically recrystallized feldspar is present throughout the sample and exhibits both BLG and SGR recrystallization in the C and S domains respectively.

4.2 *EBSD Maps of WMSZ-188*

4.2.1 *EBSD Maps Introduction*

Three EBSD maps of sample WMSZ-188 were created: two from site 1 (maps 1a and 1b, Fig. 4), and one from site 2 (map 2, Fig. 4). The maps are colored based on their Euler angle. Euler angles are chromatic indicators of crystallographic orientation. The EBSD maps of sites 1a and 2 contain grains that are distinctly larger on the right side of the map than the left side. There is also a higher incidence of zero solutions, or not indexed points, on the left side of these maps than the right. This circumstance is likely due to a decrease in grain size that results in a higher concentration of grain boundaries and an increase in lattice distortion in the areas that are more highly deformed. The high quantity of zero-solution points on the left side of these maps alters the apparent size of the grains, making them appear smaller than they are. Thus, meaningful grain-size analyses are not possible with these data.

Misindexed points within grains also cause problems with data analyses. Some individual grains contain anomalous zero-solution data points that create 90° spikes in the misorientation profiles. These anomalous spikes were removed

in the grain boundary maps by excluding their misorientation values (90 ± 5°). Similar spikes are created by points misindexed as Dauphiné twins, which have apparent misorientations of 60° about the *c*-axis. Dauphiné twins occur when quartz goes through the beta quartz to alpha quartz polymorph transition (Menegon et al., 2011). However, evidence of Dauphiné twinning should have been destroyed when the quartz was dynamically recrystallized below the beta-alpha transition. The points indexed as Dauphiné twins are also randomly distributed throughout the individual quartz grains. Therefore, they are probably the result of an indexing error (Menegon et al., 2011).

4.2.2 *EBSD Map of Site 1a*

The map of site 1a consists of an x-y grid of 674 by 182 data points (122,668 data points total). The average MAD is 0.6694 with 77.4 % of the data points indexed as quartz. The map is located in the C domain and the transition zone between the C and S domains of site 1 (Fig. 5). The quartz grains in the C domains are elongate parallel to C foliation, and the quartz grains in the S-C transition zone are elongate parallel to the S foliation. There are two areas in the bottom of the map area that are not indexed because there are flaws in the thin section (Fig. 10).

Grains were selected for isolation and individual analyses based on grain-size and position in the map area. The seven largest grains range in area from 81,392–6,328 μm^2 and they are evenly distributed on the right two-fifths of the map. This division was made based on the change from what appears to be S-C transition zone to the C domain. Only five of these large grains were analyzed

separately because two of the grains extend out of the map area in two directions; these grains are labeled b, c, d, e, and f (Fig. 10). Three of the five grains analyzed also extend out of the map area; however, it is only in one direction. The five, large, grains were mapped and analyzed separately using a texture-component map that allowed for 20° internal misorientation (Fig. 10b-f).

Internal misorientation varies depending on the quartz grains' proximity to the C or S domain. The larger grains farther to the left in the map area, closer to the C domain, exhibit more internal misorientation than the grains on the right side, closer to the S domain (Fig. 10). The elongate grains (b and c), in particular, have high internal misorientation values (10-20°). These zones of internal misorientation are inclined in the direction of the long axis of the grains and the C foliation, sympathetic with the shear direction. However, there are zones of internal misorientation within grains d, e, and f that are gradients of 0° to ~7° of misorientation (Fig. 10). These grains (d, e, and f) have larger cores of low misorientation, with rounded to sub-rounded areas of internal misorientation at some points on their edges, but these areas do not extend all around the grain. Some of the gradients of internal misorientation, especially in grain e, are very slight and undulose. These zones of internal misorientation seen in the S domains are very similar to the extinction patterns in the island grains in WMSZ-065 and -069 (Figs. 8, 10).

Seven grains were selected for internal misorientation analyses on the left three-fifths of the map (b-h). These grains were selected because they are large enough in area for analyses (988–752μm^2) and evenly distributed across the left-

hand portion of the map area (Fig. 11). More small than large grains were analyzed in this section of map 1a because of their relative abundance. These grains are elongate parallel to the C foliation and all exhibit a core with little internal misorientation; however, the ends of the long axes of these grains have some rounded areas of internal misorientation. These areas are defined by very slight internal misorientations that are not easily distinguished from one another (Fig. 11). Subgrains occur around portions of the periphery of the small grains. The misorientations across the boundaries of these grains are all relatively high (~ 20–88°).

4.2.3 *EBSD Map of Site 1b*

The map of site 1b is an x-y grid of 498 by 476 data points (237,048 points total) with an average MAD of 0.7079 and 81.62% of the points are indexed as quartz. The map is located in the S domain of site 1 (Fig. 5). The area of zero solutions (upper right-hand portion of the map area) is a biotite crystal. Site 1b is in the S domain of the mylonite where the quartz grains are large with distinct lobate and amoeboid grain boundaries (Figs. 5, 12). Here, there is evidence of grain consumption including the presence of relict and island grains which all have the same orientation as their original, neighboring parent grain (Figs. 6, 9). Six grains in map 1b were isolated for individual analyses. The texture-component maps created for these grains show that less internal deformation occurs in the grains farther from the C domains (i.e., farther to the right of site 1a) (Fig. 12). Representative 2-D misorientation profiles taken across grain boundaries show large, abrupt changes in orientation (Fig. 13). In each case,

there is at least 32° of misorientation across the grain boundaries and at most ~90° of misorientation. This degree of misorientation occurs over 5 μm or less in all analyzed grains (Fig. 13). There are zones of internal misorientation around the edges of the grains, but this is much less pronounced than in the grains from site 1a. The grain in Figure 12g exhibits rounded areas with slightly different orientations in the upper portion of the grain. Other grains show a more gradual shift in internal orientation moving from the center of the grains towards the edges but general areas of internal misorientation still exist (Figs. 12c-f).

4.2.4 *EBSD Map Site 2*

The map of site 2 is an x-y grid of 475 by 349 data points (165,775 total). The average MAD is 0.6324 with 78.01% of the data points indexed as quartz. The map is located in the C domain and the transition zone between the C and S domains (Fig. 14). The large, mostly blank area (lower left-hand corner) is recrystallized feldspar (Fig. 15). Map 2 exhibits similar grain-size distribution and internal misorientation trends as observed in map 1a (Figs. 10, 15). Towards the C domain (left-side of the map), grain-size significantly decreases. The misorientation across grain boundaries is relatively high across the entire map area (>10°). The larger grains closer to the S domains exhibit some zones of internal misorientation in the texture-component maps (Fig. 15), similar to that found in the right-hand portion of map 1a and most of map 1b. There is a lower incidence of zero solutions on the left side of the map, where the grains get smaller than in map 1a. There is a higher incidence of the false Dauphiné twins within some of the larger grains than in map 1a, which causes grain detection to

be inaccurate. Because of this, the grains picked by the HKL software are too skeletal for internal misorientation analyses.

4.2.5 *Quartz CPOs in Maps 1a and 2*

The crystallographic preferred orientations (CPO) of quartz measured in maps 1a and 2 evaluate the fabric strength and the dominant slip systems that were active (Fig. 16- only map 1a plotted). The single-girdle fabric with two *c*-axis maxima separated by 60° indicates that rhomb-slip dominated in the C domain (Fig. 16). Rhomb-slip is typical of increasing temperatures in quartz (Tullis, 2002). The *c*-axis and *a*-axis maxima are both slightly off centered. This is likely because the thin section was not cut perfectly perpendicular to the local flow plane and perfectly parallel to the local slip direction in these domains. Due to the small number of grains mapped in the S domains, no definitive CPO could be determined.

5. Interpretations

5.1 *Recrystallization mechanisms—WMSZ-188*

The EBSD maps of WMSZ-188 can be divided into areas of SGR-dominated recrystallization generally corresponding to the C domains, GBM-dominated recrystallization generally corresponding to the S domains, and SGR-GBM recrystallization transition zones between the C and S domains. The quartz grains in the C domains exhibit SGR-dominated recrystallization because of: their smaller relative grain size; blurry, indistinct grain boundaries; and subgrain formation around the periphery of the grains. The quartz grains in the S domains exhibit GBM-dominated recrystallization because of: their large lobate, amoeboid

grain shape; formation of island grains; and high-angle grain boundaries (>20°). The quartz grains in the zone of transition from C to S domains exhibit SGR-GBM recrystallization because of their moderate grain size and their stronger development of internal misorientation and subgrains than in the S domains.

5.2 *Deformation temperature*

The presence of GBM recrystallization of quartz and BLG recrystallization of feldspar in sample WMSZ-188, indicate that WMSZ-188 was deformed under upper-greenschist-facies to lower-amphibolite-facies temperatures, assuming "normal" strain rate. It is likely that temperatures remained high during deformation because of the syndeformational emplacement of the Boundary Peak pluton. Several lines of evidence support this claim. First, feldspars in both the C and S domains, are dynamically recrystallized. The presence of recrystallized feldspars indicates that the entire sample must record temperatures high enough for dynamic recrystallization, > 500 °C at "normal" strain rates (Paschier and Trouw, 2005). In addition, the absence of any chlorite replacement of biotite indicates that the sample did not recrystallize at temperatures below ~ 400 °C (Spear, 1992). Finally, the quartz CPOs identified in maps 1a and 3 indicate rhomb slip, which occurs from ~450 to 600 °C (Tullis, 2002; Paschier and Trouw, 2005).

5.3 *Coeval recrystallization mechanisms*

There are four lines of evidence that support the cotemporaneous operation of SGR and GBM recrystallization in quartz in sample WMSZ-188:

- Firstly, the three EBSD maps all reveal high-angle grain boundaries in both the C and S domains. The presence of high-angle grain boundaries in C domains exhibiting a microstructure indicative of SGR recrystallization is likely due to prolonged deformation resulting in continuous grain rotation, further increasing their misorientation (Halfpenny et al., 2006). If the SGR recrystallization occurred during a second deformational event and the SGR-dominated grains were rotated to the degree present in the sample, it is highly unlikely that the grains in the S domains would be recrystallized via GBM recrystallization— especially in the single quartz ribbon that extends between domains (Fig. 2). The presence of high-angle grain boundaries in the SGR domains is also inconsistent with the subgrain rotation model that suggests there should be a gradual shift in orientation across grain boundaries (Halfpenny et al., 2006). Hence, the moderate abundance of high-angle boundaries in the SGR-dominated domains also could record relatively minor GBM recrystallization in the C domains.
- Secondly, there is no evidence of a significant SGR recrystallization over-print in the GBM-dominated areas. The texture-component maps (Figs. 7, 9, 12), created from the quartz EBSD data in the S domains, illustrate zones of internal misorientation. These could be construed as evidence for SGR recrystallization over-printing during a second deformation event; however, it is more likely that these zones of internal misorientation formed spontaneously during grain growth and enhanced during

deformation. During GBM recrystallization under static stress conditions, grains develop slight (1–2°) misorientations because of impurities or missing atoms that cause slight kinks in the crystal lattices (Piazolo et al., 2005). These slight imperfections serve as catalysts for subgrain formation under static stress conditions (Piazolo et al., 2005). Therefore, quartz grains that form during GBM-dominated dynamic recrystallization should have some internal misorientation. Subsequently, if deformation occurs while the grains are forming, or have formed, the zones of internal misorientation become more apparent because they will trap dislocations. Additionally, it is possible for a grain undergoing GBM recrystallization to consume a grain that was subjected to SGR recrystallization and, thus, contain its misoriented, subgrain-like, appearance, without being affected by SGR itself (Bestmann et al., 2005). Therefore, the degree of internal misorientation seen in the GBM-dominated areas of WMSZ-188 can develop during GBM recrystallization and is not necessarily a reflection of a SGR recrystallization over-print. These results indicate that the definitions of a subgrain, using both Simpson's (1998) and Pachier and Trouw's (2005) definitions, does not necessarily indicate how the subgrain was generated; thus the presence of subgrains in quartz in the S domains is insignificant for the purposes of this study.

- Third, the quartz ribbon that traverses the C and S domains is a strong indicator of coeval recrystallization mechanisms (Fig. 2). Because nothing shields the part of the quartz ribbon in the S domain from any sort of late-

stage, low temperature deformation, the only way the two recrystallization mechanisms could have formed is by synchronous recrystallization in the two domains.

- Lastly, the preservation of features that record relatively high temperature deformation such as recrystallized feldspars, CPOs indicative of rhomb slip, and the lack of biotite replacement suggest that recrystallization mechanisms were operating simultaneously, and that the localized SGR recrystallization is not an artifact of late-stage, lower-temperature deformation.

5.4 *Regional support for coeval recrystallization mechanisms*

Regionally, there is a strong correlation between the amount of quartz in a sample and the dominant recrystallization mechanism. Samples WMSZ-065 and 103 were deformed at approximately the same distance from the Boundary Peak pluton. WMSZ-065 has a high quartz content and is dominated by GBM recrystallization, whereas WMSZ-103 has a low quartz content and is dominated by SGR recrystallization. Because quartz is the rheologically weaker mineral in these samples, it deforms more easily and is subjected to higher strain rates. Thus, in WMSZ-188, which has relatively moderate feldspar content, both recrystallization mechanisms can operate.

Samples WMSZ-065 and 069 also provide evidence to support coeval recrystallization mechanisms. These record GBM recrystallization of quartz with extinction patterns that are strikingly similar to the internal misorientation patterns recorded in the GBM-dominated grains in all three of the EBSD maps of WMSZ-

188 (Figs. 8, 12). The strong resemblance of the texture-component maps to the pure GBM recrystallized quartz extinction patterns indicates that the zones of internal misorientation are not a reflection of SGR recrystallization overprint and they can exist in mostly strain-free GBM recrystallized quartz grains (Figs. 8, 12). The connection between optical extinction patterns and the misorientations of the internal structure of recrystallized quartz grains could not have been noticed without detailed mapping resulting from EBSD analyses.

Comparison of samples WMSZ-103, WMSZ-065, and WMSZ-188 indicates that the dominant recrystallization mechanism is not correlated with distance from the Boundary Peak pluton, but that it is correlated with the quartz content— low quartz samples exhibit more SGR recrystallization. This suggests that the transition between SGR and GBM in these samples is a temperature independent process. Therefore, the only other variable that can account for the different recrystallization mechanisms is a domainal variation in strain rate driven by the concentration of quartz in through-going networks.

6. Broader Implications

6.1 *Implications for S-C mylonite formation*

S-C mylonites form by progressive deformation that leads to propagated planes of weakness and, eventually, the formation of distinct C foliations (Snoke et al., 1998). My analyses demonstrate that the two different recrystallization mechanisms, SGR and GBM, present in the C and S domains of WMSZ-188 operated simultaneously. This sample does not record a syndeformational decrease in temperature because of the lack of any low-temperature

overprinting. These rocks probably experienced nearly isobaric deformation because of their setting in a strike-slip fault system (Sullivan and Law, 2007).

Using other studies of recrystallization mechanisms in quartz provides a basis for estimates of strain-rate partitioning in WMSZ-188. Comparing Stipp et al.'s (2002) findings on dynamically recrystallized quartz-dominated rocks from the eastern Tonale fault zone to the results of this study, enabled the estimation of maximum strain rate in sample WMSZ-188 (Fig. 17, Stipp et al., 2002). The two samples presented by Stipp et al. (2002) from the eastern Tonale fault zone that are most comparable to WMSZ-188 record deformation temperatures from ~490–510 (Stipp et al., 2002). These plot in the GBM recrystallization regime in the diagram (Fig. 17, Stipp et al., 2002). WMSZ-188 likely lies within these temperatures based on their similarities. Hirth and Tullis' (1992) experimentally derived regime-III (GBM-dominated recrystallization) is most similar to the recrystallized quartz in S domains in WMSZ-188. The grains, however smaller, also exhibit some high-angle, as well as gradational, grain boundaries. The regime-III values are in the upper left portion of the recrystallization mechanism diagram and lie on the boundary between the GBM and SGR zones.

At a constant temperature, at least an order of magnitude difference in strain rate is needed to switch between SGR and GBM recrystallization of quartz (Fig. 17, Stipp et al., 2002). The range of potential strain rates in WMSZ-188 was determined using a similar range in values as is presented by Stipp et al. (2002). The flow law equations of Luan and Patterson (1992) and Gleason and Tullis (1995) are accepted as the most accurate equations (Tullis, 2002). The transition

of one dominant recrystallization mechanism to another, at a constant temperature, could require one to three orders of magnitude of change in strain rate (Fig. 17, Stipp et al., 2002).

The major implications for this domainal strain-rate partitioning are the potential for erroneous assumptions of deformation temperature. Many previous assumptions regarding the controls on recrystallization mechanisms, especially deformation temperature, and how they are manifested in plastically deformed fault rocks may require reexamination (Lister and Snoke, 1984; Hirth and Tullis, 1992; Zulaf, 2001; Tullis, 2002; Stipp et al., 2010).

6.2 *Other S-C mylonites that exhibit transitional recrystallization mechanisms*

Behr and Platt (2011) described an S-C mylonite with very similar fabric patterns to those identified in WMSZ-188. Their study investigated the presence of different recrystallization mechanisms in rocks deformed in an extensional shear zone. They assumed varying temperatures and pressures based on the heat transfer equation in two dimensions for a rolling hinge fault geometry (Behr and Platt, 2011). Deformation temperatures were determined using Ti concentrations in quartz; however this technique is not completely reliable for SGR recrystallization (Gruijk et al., 2011). Behr and Platt (2011) suggest that the different recrystallization mechanisms that operated in the fault system were caused by a decrease in temperature and pressure during exhumation. However, my data illustrate that the same spatial variations in recrystallization mechanisms can develop in a sample that was deformed in a system that potentially records relatively constant confining pressure and no syn-tectonic temperature decrease.

Therefore, spatial strain-rate variations must be considered when using quartz recrystallization mechanisms to analyze variations in deformation temperature.

7. Conclusion

The S and C domains of WMSZ-188 were subjected to different strain rates, which allowed two different recrystallization mechanisms to operate simultaneously during deformation; SGR recrystallization occurred in the C domains while, concurrently, GBM recrystallization occurred in the S domains. This fabric commonly is interpreted as resulting from temperature decrease over the course of deformation. However, this study presents data from a sample deformed under relatively isothermal conditions that exhibits two coeval, domainal, recrystallization mechanisms. The transition from one recrystallzation mechanism to another (SGR to GBM or GBM to SGR) requires one to three orders of magnitude of change in strain rate (Stipp et al., 2002). This high magnitude of strain-rate partitioning occurred between the C and the S domains in sample WMSZ-188.

References

Behr, W.M., and Platt, J.P., 2011, A naturally constrained stress profile through the middle crust in an extensional terrane: Earth and Planetary Science Letters, v. 303, p. 181-192.

Bestmann, S. Piazolo, C., Spiers, C., and Prior, D. J., 2005, Microstructural development of rocksalt during in-situ heating experiments: Journal of Structural Geology, v. 27, p. 447-457.

Biswal, T.K., Thirukmaran, V., Ratre, K, Bandyapadhaya, K., Sundaralingam, K., and Mondal, A. K., 2010, A study of mylonites from parts of the Salem-Attur shear zone (Tamil Nadu) and its tectonic implications: Journal of the Geological Society of India, v. 75, p. 128-136.

Corsini, M., Vauchez, A., and Caby, R., 1996, Ductile duplexing at a bend of a continental-scale strike-slip shear zone: example from NE Brazil: Journal of Structural Geology, v. 21, p. 385-394.

Crowder, D.F., Robinson, P.F., Harris, D.L., 1972, Geologic map of the Benton quadrangle Mono County, California and Esmeralda and Mineral Counties, Nevada. U.S. Geological Survey Map GQ-1013, scale 1: 62,500.

Crowder, D.F., McKee, E.H., Ross, D.C., Krauskopf, K.B., 1973, Granitic rocks of the White Mountains area, California-Nevada: age and regional significance: *Geological Society of America Bulletin*, v. 84, p. 285-296.

Fynn, G.W., Powell, W.J.A., 1979. The Cutting and Polishing of Electro-optic Materials. Adam Hilger, London, 216 pp.

Gleason, G.C. and Tullis, J., 1995, A flow law for dislocation creep of quartz aggregates determined with the molten salt cell: *Tectonophysics*, v. 247, p. 1-23.

Halfpenny, A., Prior, D.J., Wheeler, J., 2006, Analysis of dynamic recrystallization and nucleation in a quartzite mylonite: Tectonophysics, v. 427, p. 3-14.

Hirth G., Tullis, J., 1992, Dislocation creep regimes in quartz aggregates: Journal of Structural Geology, v. 14, p. 145-160.

Jain, A.K and Manickavasagam, R.M., 1993, Inverted Metamorphism in the intracontinental ductile shear zone during Himalayan collision tectonics: Geology, v. 21, p. 407-410.

Lister, G.S., and Snoke, A.W., 1984, S-C Mylonites: Journal of Structural Geology, v. 6, p. 617-638.

Lloyd, G.E., Freeman, B., 1991, SEM electron channeling analysis of dynamic recrystallization in a quartz grain: Journal of Structural Geology, v. 13, p. 945-953.

Lloyd, G.E., Freeman, B., 1994, Dynamic recrystallization of quartz under greenschist conditions: Journal of Structural Geology, v. 16, p. 867-881.

Lopes, A.E.V., Assumpção, M., do Nascimento, A.F., Ferreira, J.M., Menezes, E.A.S., and Barbosa, J.R., 2009, Intraplate earthquake swarm in Belo Jardim, NE Brazil: reactivation of a major Peoproterozoic shear zone (Pernambuco Lineament): Geophysical Journal International, v. 180, p. 1303-1312.

Luan, F.C. and Patterson, M.S., 1992, Preparation and deformation of synthetic aggregates of quartz: *Journal of Geophysical Research*, v. 97, p. 301-320.

McKee, E.H., and Conrad, J.E., 1996, A tale of 10 plutons, revisited: Age of granitic rocks in the White Mountains, California and Nevada*: Geological Society of America Bulletin*, v. 108, p. 1515-1527.

Menegon, L., Piazolo, S., and Pennacchioni, G., 2011, The effects of Dauphiné twinning on plastic strain in quartz: Contributions to Mineralogy and Petrology, v. 161, p. 635-652.

Passchier, C. W. and Trouw, R.A.J., 2005, *Microtectonics*: Berlin, Springer, p. 42-43, 121-123.

Piazolo, S., Prior, D.J., and Holness, M.D., 2005, The use of combined cathodoluminescence and EBSD analysis: a case study investigating grain boundary migration mechanisms in quartz: *Journal of Microscopy*, v. 217, p. 152-161.

Prior, D.J, Mariani, E., and Wheeler, J., 2009, EBSD in the Earth Sciences: Applications, Common Practice, and Challenges: In: Schwatrz, A. Kumar, M., Adams, B.L., and Field, D.P., 2009, *Electron Backscatter Diffraction in Materials Science,* Springer*,* p. 346-360.

Schmid, S.M. and Casey, M., 1986, Complete fabric analysis of some commonly observed c-axis patterns: Geophysical Monograph, v. 36, p. 263-286.

Schmidt, N.H., and Olesen, N.O.,1989, Computer-aided determination of crystal-lattice orientation from electron channeling patterns in the SEM: *Canadian Mineralolgist*, v. 27, p. 15-22.

Snoke, A.W., Tullis, J., and Todd, V.R., 1998, Fault-Related Rocks: A Photographic Atlas: Princeton, Princeton University Press, p. 5-6.

Spear, F. S., 1994, Metamorphic Phase Equilibria and Pressure-Temperature-Time Paths. Monograph of the Mineralogical Society of America. 799 p.

Stipp, M., Holger, S., Hielbronner, R., and Schmid, S.M., 2002, Dynamic recrystallization of quartz: correlation between natural and experimental conditions: In: De Meer, S., Drury, M.R., de Bresser, M.H.P., and Pennock, G.M. (eds.), 2002, Deformation Mechanisms, Rheology, and Tectonics: Current Status and Future Perspectives: Geological Society, London, Special Publications, v. 200, 171-190 pp.

Stipp, M., Tullis, J., Scherwath, M., and Behrmann, J.H., 2010, A new perspective on paleopiezometry: Dynamically recrystallized grain size distributions indicate mechanism changes: Geology, v. 38, p. 759-762.

Stipp, M., Stünitz, H., Heilbronner, R., Schmid, S.M., 2002, Dynamic Recrystallization of quartz: correlation between natural and experimental conditions. In: de Meer, S., Drury, M.R., de Bresser, J.H.P., Pennock, G.M. (Eds.), Deformation Mechanisms, Rheology and Tectonics: Current Status and Future Perspectives. Geological Society, London, Special Publication, v. 200, p. 171-190.

Sullivan, W.A., 2003, “Geometry, kinematics and age of the northern half of the White Mountain shear zone, eastern California and Nevada.” M.S. Thesis, Virginia Polytechnic Institute, Blacksburg, VA.

Nzenti, J.P., Kapajika, B., Woerner, G., and Lubala, T.R, 2006, Synkinematic emplacement of granitoids in a Pan-African shear zone in central Cameroon: Journal of African Earth Sciences, v. 45, p. 74-86.

Sullivan, W.A. and Law, R.D., 2007, Deformation path partitioning within the transpressional White Mountain shear zone, California and Nevada: Journal of Structural Geology, v. 29, p. 583-598.

Sullivan, W.A., and Bean, R.J., 2010, Asymmetrical quartz crystallographic fabrics formed during constructional deformation: *Journal of Structural Geology*, v. 32, p. 1430-1443.

Trimby, P.W., Prior, D.J., Wheeler, J., 1998, Grain boundary hierarchy development in quartz mylonite: Journal of Structural Geology, v. 20, p. 917-935.

Tullis, J., 2002, Deformation of Granitic Rocks: Experimental Studies and Natural Examples: In: Karato, S., and Wenk, H. (eds.), 2002, Reviews in Mineralogy & Geochemistry,v. 51, 51-95 p.

Tullis, J., and Yund, R.A., 1985, Dynamic recrystallization of feldspar: A mechanism for ductile shear zone formation: *Geology*, v. 13, p. 238-241.

Tullis, J., and Yund, R.A., 1992, Experimental evidence for diffusion creep in feldspar aggregates: *Journal of Structural Geology*, v. 13, p. 987–1000.

van Daalen, M., Heilbronner, R., Kunze, K., 1999, Orientation analysis of localized shear deformation in quartz fibers at the brittle-ductile transition: Tectonophysics, v. 303, p. 83-107.

Wang, C. and Ludman, A., 2004, Deformation conditions, kinematics, and displacement history of shallow crustal ductile shearing in the Norunbega fault system in the Northern Appalachians, eastern Maine: *Tectonophysics*, v. 384, p. 129-148.

Figure Captions

Figure 1. Stability fields of quartz recrystallization mechanisms in strain rate-temperature space. (Stipp et al., 2002). Stipp et al.'s data are plotted with three different flow law equation values for each sample. Hirth and Tullis (1992) determined stability fields for recrystallization mechanisms in quartz in experimentally deformed rocks. These values are displayed on the diagram in gray.

Figure 2. Photomicrograph of recrystallized quartz ribbon that extends from one C domain to another, crossing an entire S domain. Taken under cross-polarized light with gypsum plate.

Figure 3. Geologic map of the northern part of the WMSZ with sample localities. Figure adapted from Sullivan and Law (2007).

Figure 4. Scanned image of the thin section of sample WMSZ-188 with sites 1 and 2 denoted. Thin section is 25 x 45 mm.

Figure 5. Photomicrograph of site 1 of sample WMSZ-188 under cross-polarized light at 20x magnification. EBSD map areas 1a and 1b are denoted by boxes.

Figure 6. (a) Photomicrograph of sample WMSZ-188 under cross-polarized light that exhibits BLG recrystallization of feldspar in a C domain (1 and 2) (b) Photomicrograph of sample WMSZ-188 in cross-polarized light that shows subgrain formation in feldspar in the S domain (3 and 4) and myrmekite growth (5).

Figure 7. (a) Photomicrograph of sample WMSZ-065 under cross-polarized light. Quartz exhibits the distinct GBM recrystallization texture of amoeboid, lobate grains (b-e) and island grains (c, d) within larger grains. Correlated with Figure 8; biotite grain in center for correlation with Figure 7.

Figure 8. (a) Photomicrograph of sample WMSZ-065, with stage rotated ~15 relative to Figure 7. Cross-polarized light shows the sweeping undulose extinction in the recrystallized quartz grains delineated in Figure 7 (b-e). The zones of undulose extinction created by internal misorientation alter the appearance of the grains with respect to Figure 7. Note that these grains are partially consumed by a larger, relatively strain-free grain. Biotite grain in center for correlation with Figure 8.

Figure 9. Photomicrograph of sample WMSZ-103 under cross-polarized light. Boxes highlight the transitional quartz recrystallization mechanisms.

Figure 10. (a) EBSD map 1a with band contrast and all Euler angles. (b-f) Quartz grains isolated for individual analyses from the right 2/5 of the map area. Texture

component maps in the upper portion of the figure illustrate internal misorientation within single quartz grains. Misorientation values are based on a centered point within each grain. Rainbow scale with 0–20° degrees of misorientation.

Figure 11. EBSD map 1a with quartz grains isolated for individual analyses from the left 3/5 of the map area. Texture component maps in the upper portion of the figure illustrate internal misorientation. Misorientation values are based on a centered point within each grain. Rainbow scale with 0–20° degrees of misorientation. Grains are enlarged by 200% to help visualize internal misorientation.

Figure 12. (a) EBSD map 1b with texture component maps that illustrate internal misorientation of six grains labeled b–g. Misorientation values are based on a centered point within each grain. Zones of internal misorientation highlighted in grain g. Rainbow scale with 0–20° degrees of misorientation.

Figure 13. (a) EBSD map 1b and misorientation profiles across grain boundaries. The profiles (b–e) represent the corresponding transects illustrated by the red lines. The 2-D misorientation profiles illustrate the misorientation relative to the first points, which are indicated by the red circles at the ends of each transect line. Spikes in the graphs indicate a large degree of misorientation.

Figure 14. Photomicrograph of site 2 of sample WMSZ-188 under cross-polarized light. EBSD map area 2 is denoted by a red box.

Figure 15. (a) EBSD map 2 with band contrast and all Euler angles. Euler angles are chromatic indicators of crystallographic orientation. Grains isolated for individual analyses are outlined and numbered. Texture component maps of grains isolated for individual analysis (b-d). Grains are enlarged by 200% to help visualize internal misorientation.

Figure 16. Equal-angle, lower-hemisphere projections, of the crystallographic orientations of quartz grains in maps 1a. These plots are based on one point per grain.

Figure 17. Stability fields of quartz recrystallization mechanisms in strain rate-temperature space (Stipp et al., 2002). Potential deformation temperature of sample WMSZ-188 indicated by red line.

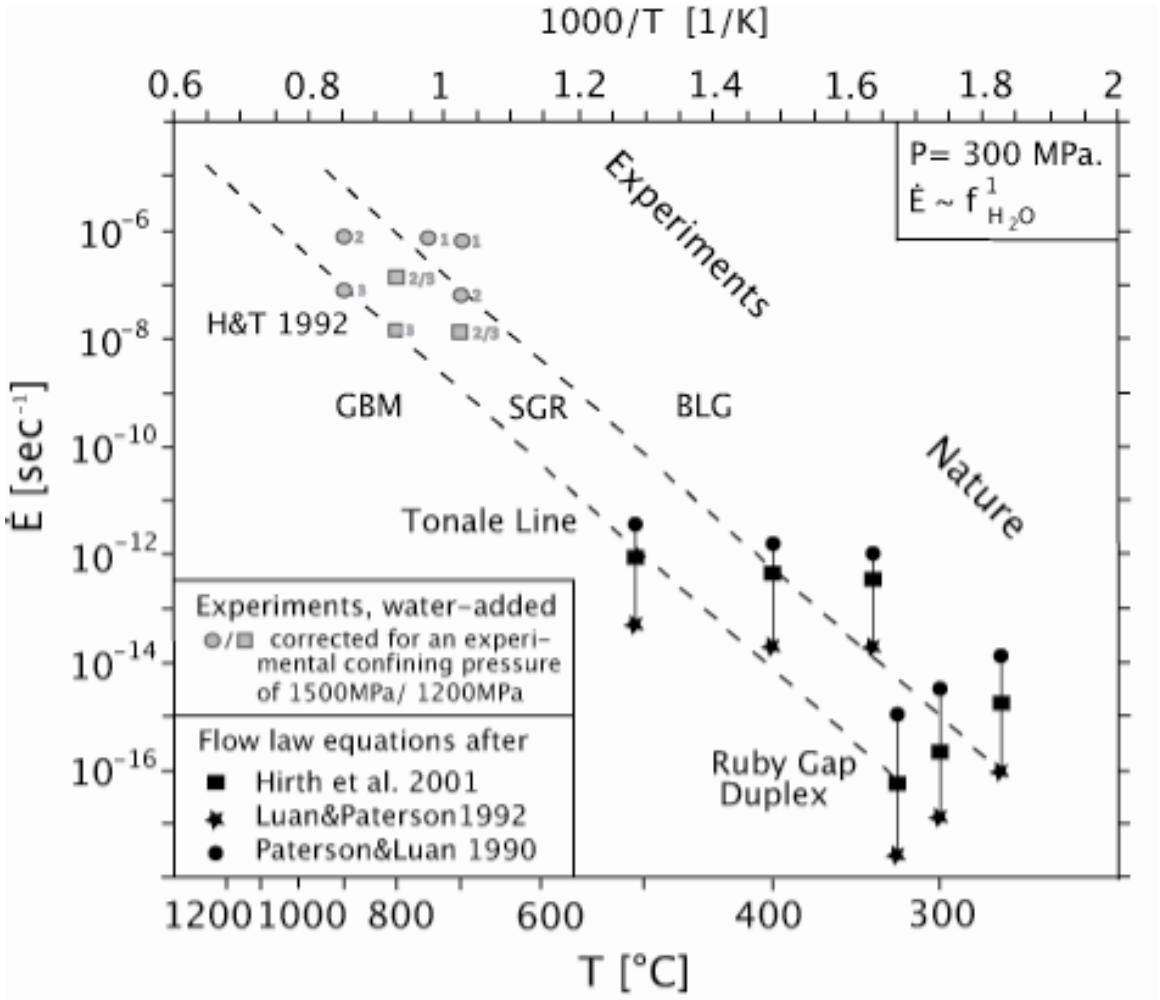
1000/T [1/K]
0.6
0.8
1
1.2
1.4
1.6
1.8
2
P= 300 MPa.
$\dot{E} \sim f^{1}_{H_2O}$
Experiments
Nature
H&T 1992
GBM
SGR
BLG
Tonale Line
Ruby Gap
Duplex
$\dot{E}$ [sec^{-1}]
10^{-6}
10^{-8}
10^{-10}
10^{-12}
10^{-14}
10^{-16}
Experiments, water-added
corrected for an experimental confining pressure of 1500MPa/ 1200MPa
Flow law equations after
Hirth et al. 2001
Luan&Paterson1992
Paterson&Luan 1990
1200
1000
800
600
400
300
T [°C]

Figure 1

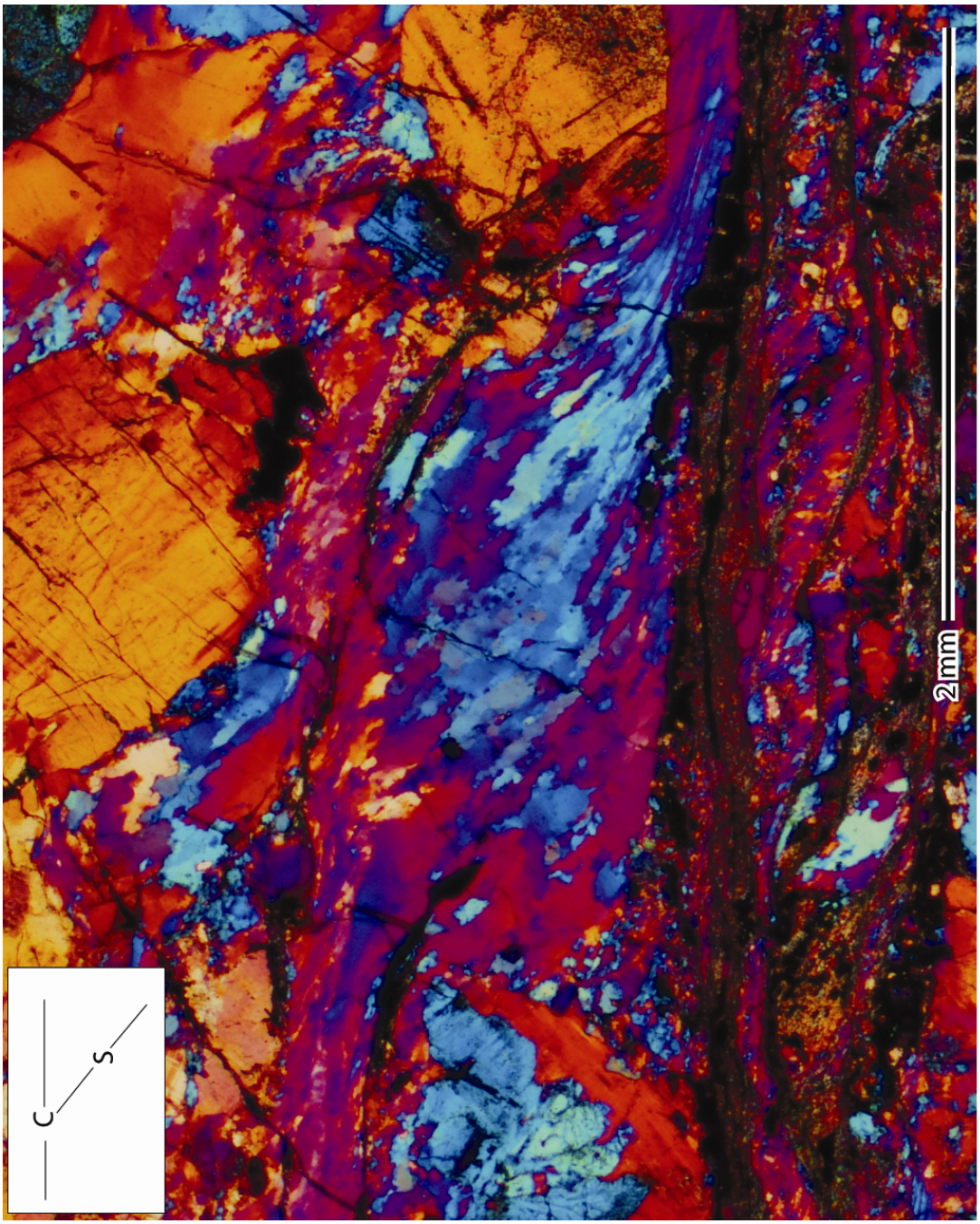

Figure 2

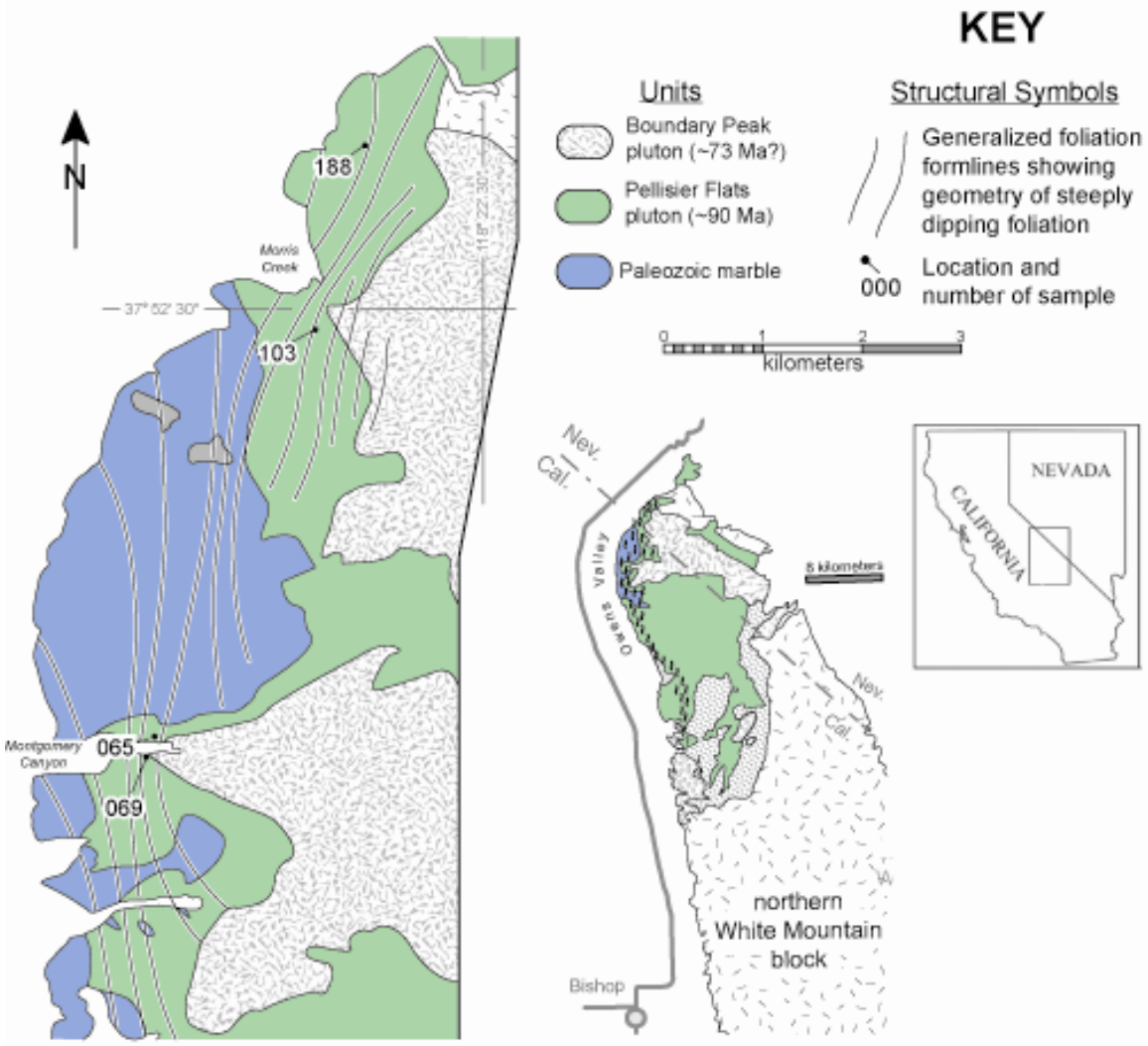
KEY
Units
Boundary Peak pluton (~73 Ma?)
Pellisier Flats pluton (~90 Ma)
Paleozoic marble
Structural Symbols
Generalized foliation formlines showing geometry of steeply dipping foliation
000
Location and number of sample
0 1 2 3
kilometers
N
188
103
065
069
Morris Creek
Montgomery Canyon
37° 52' 30"
118° 22' 30"
Nev.
Cal.
Owens Valley
5 kilometers
northern White Mountain block
Bishop
NEVADA
CALIFORNIA

Figure 3

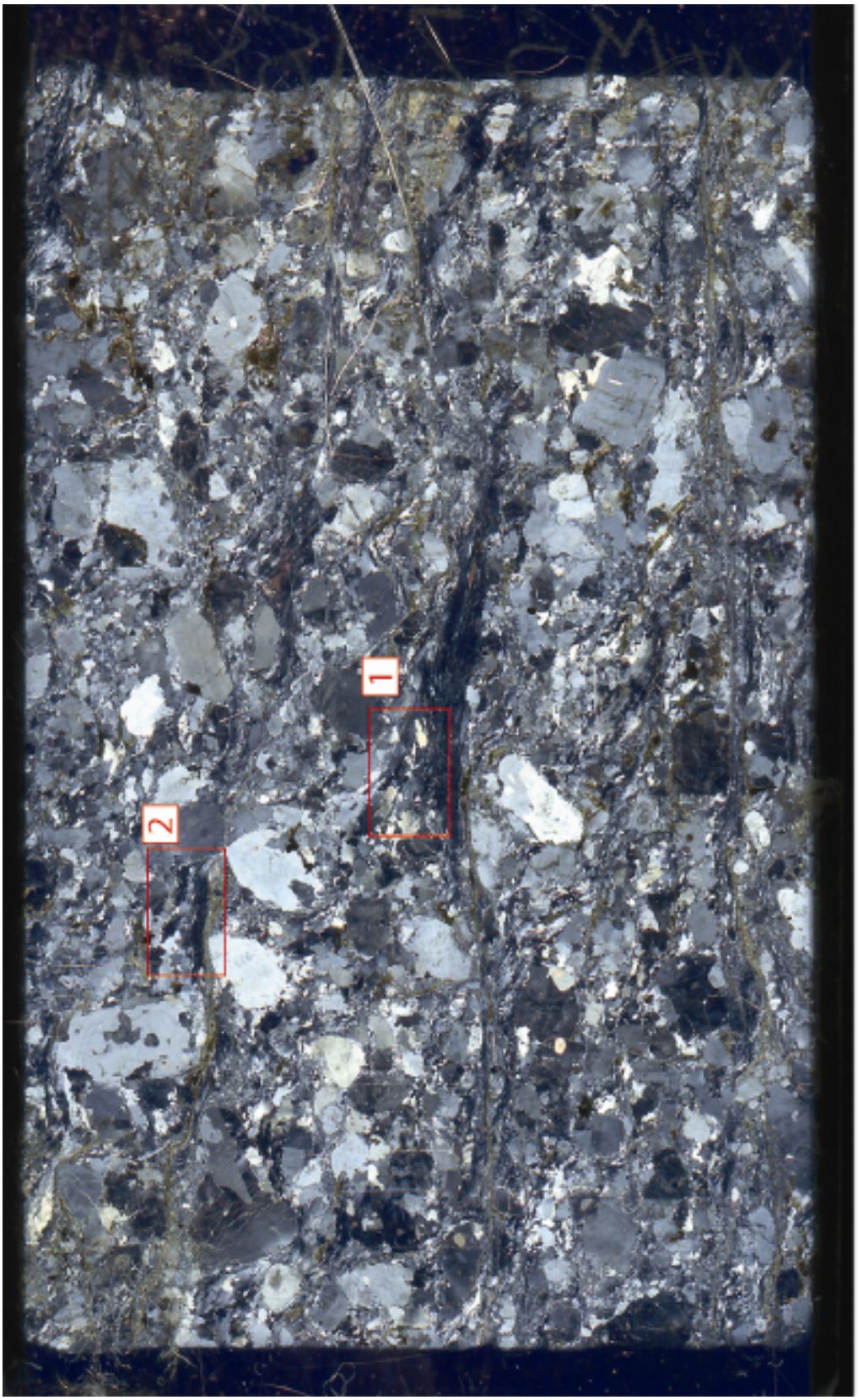

Figure 4

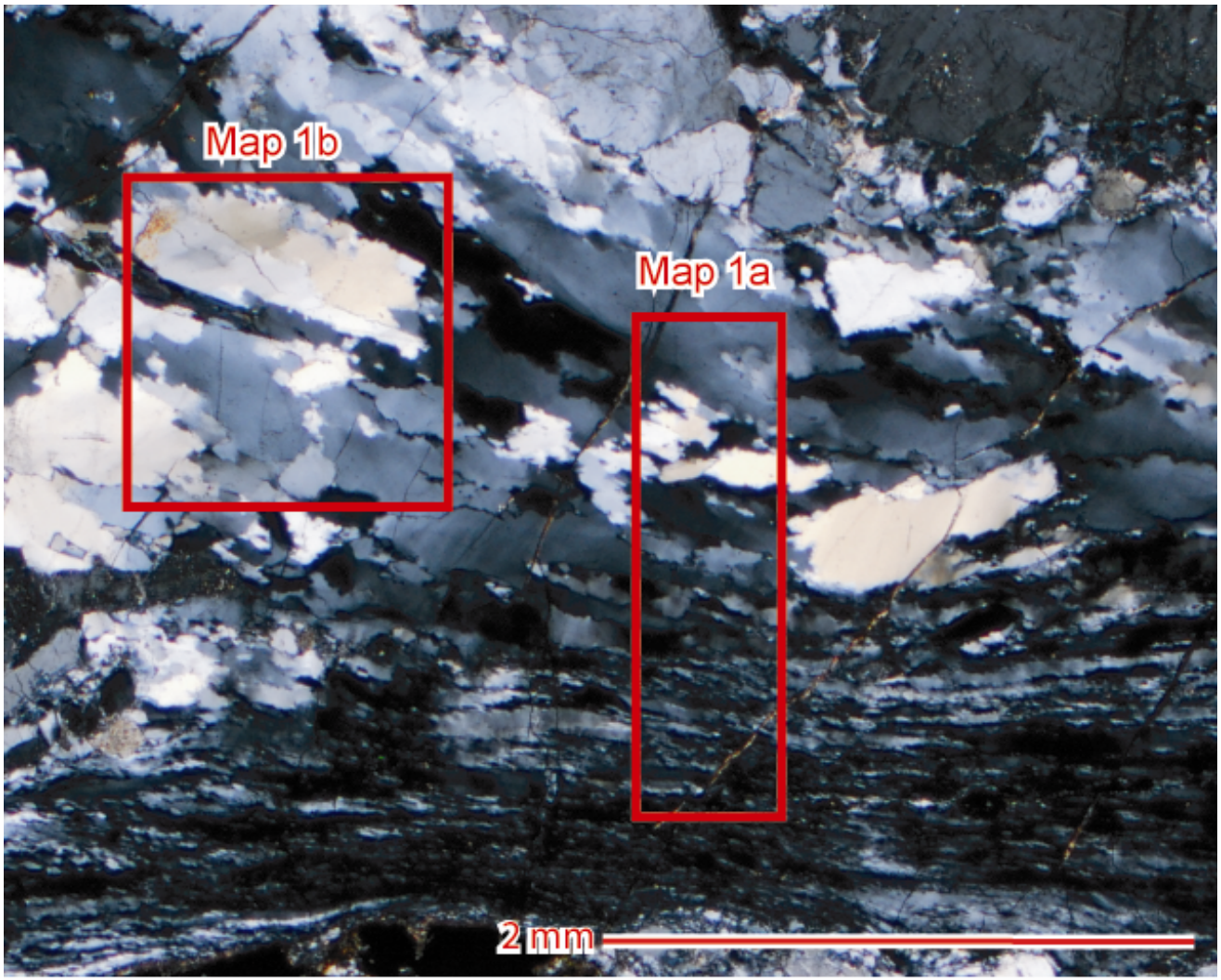

Figure 5

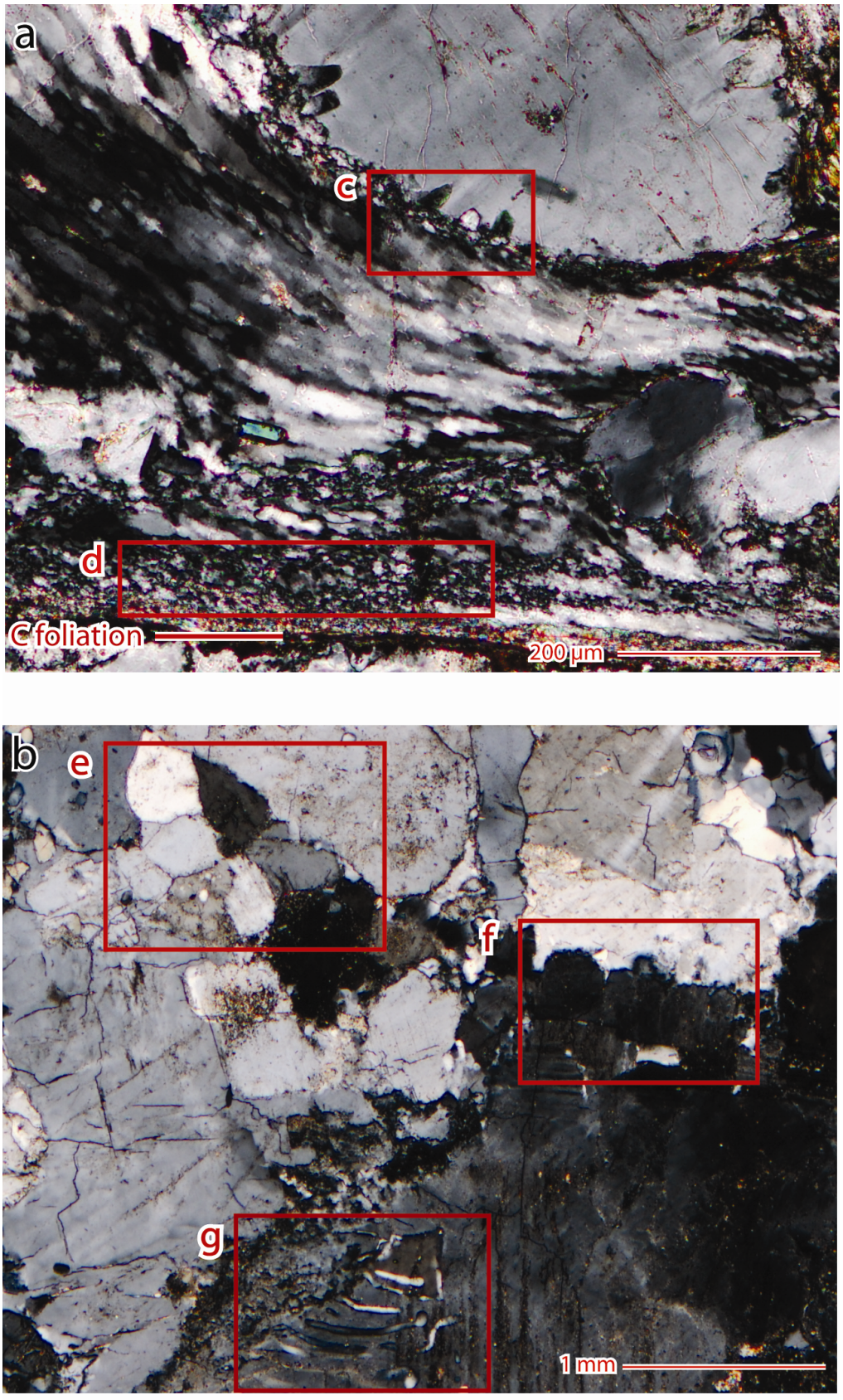

Figure 6

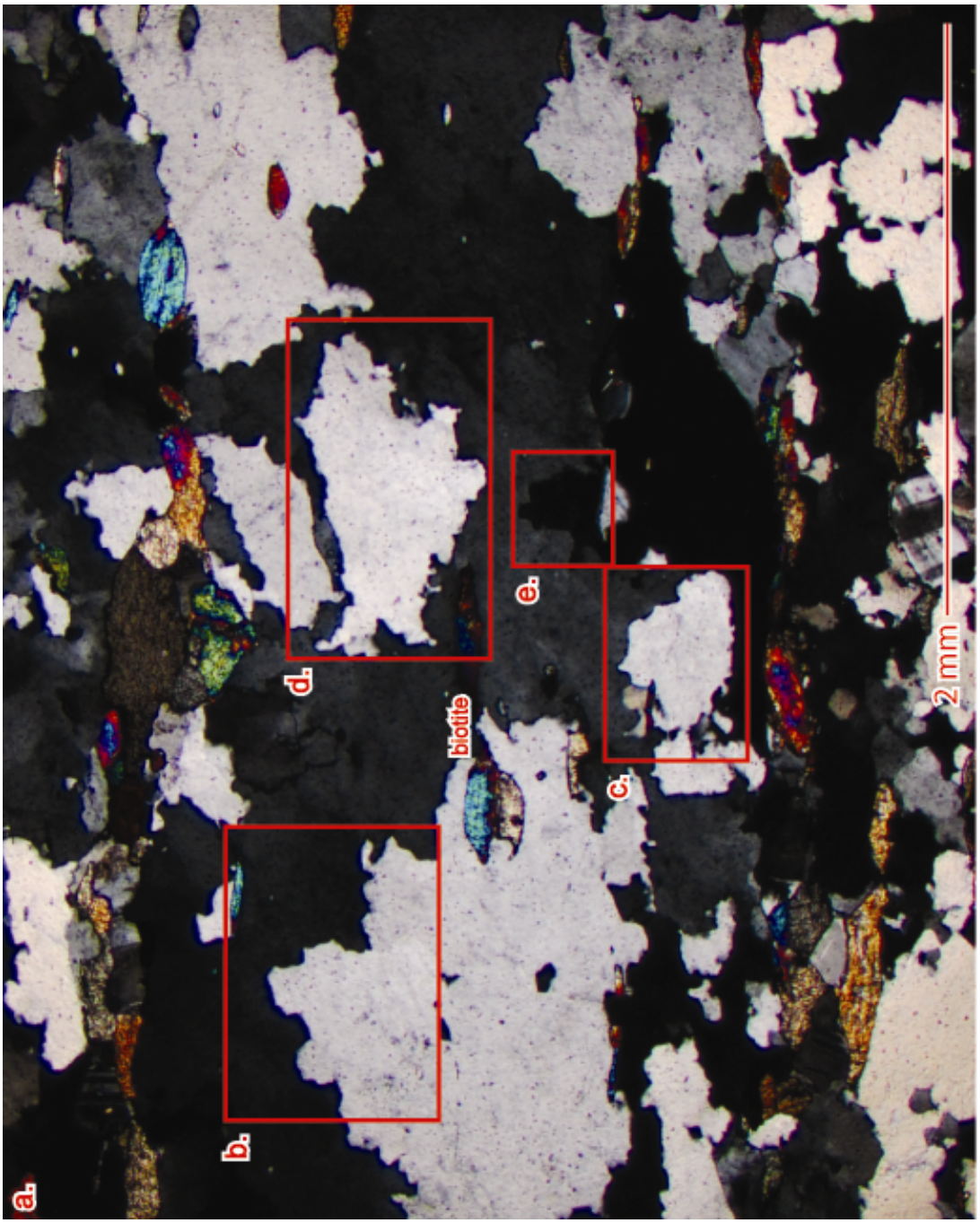

Figure 7

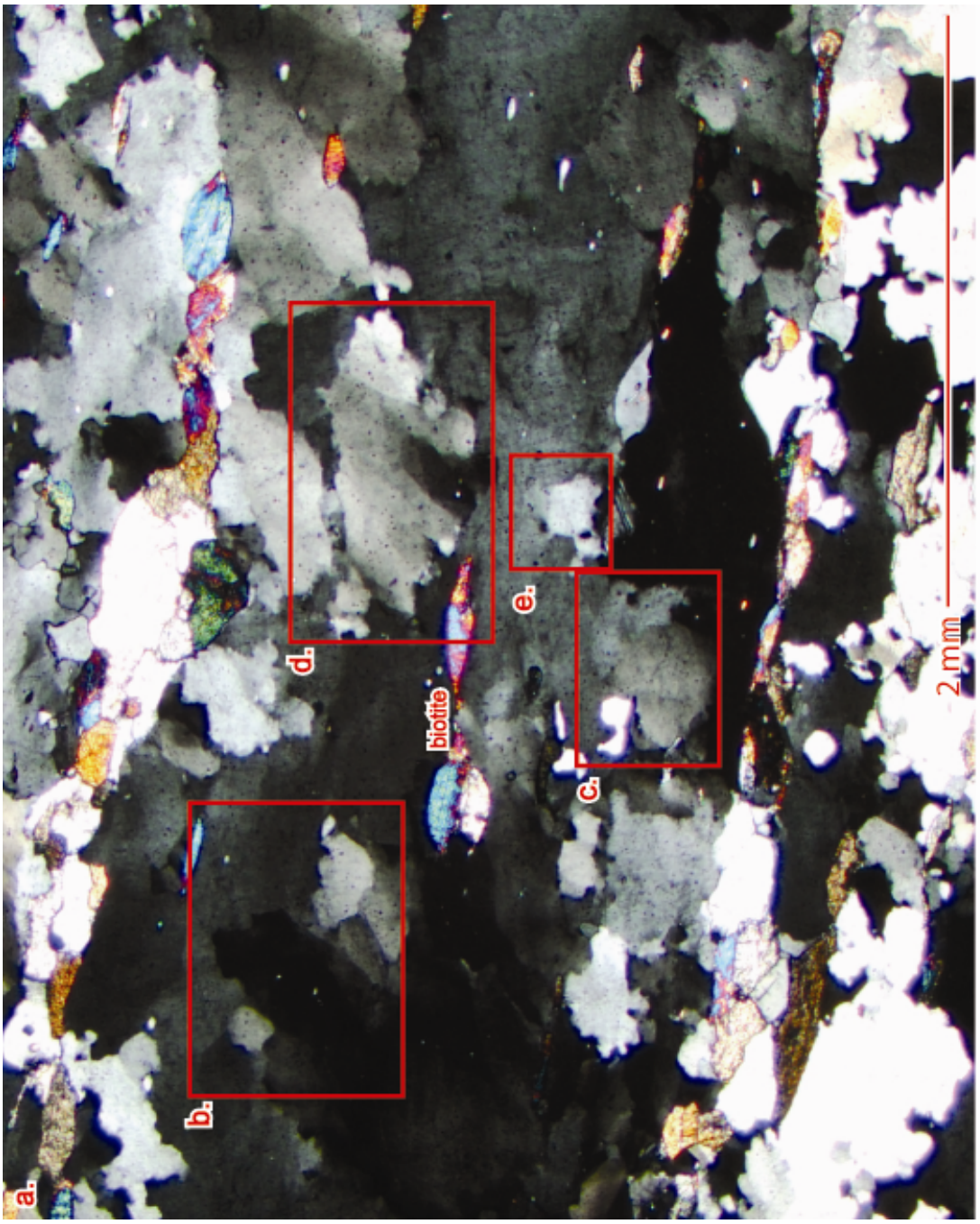

Figure 8

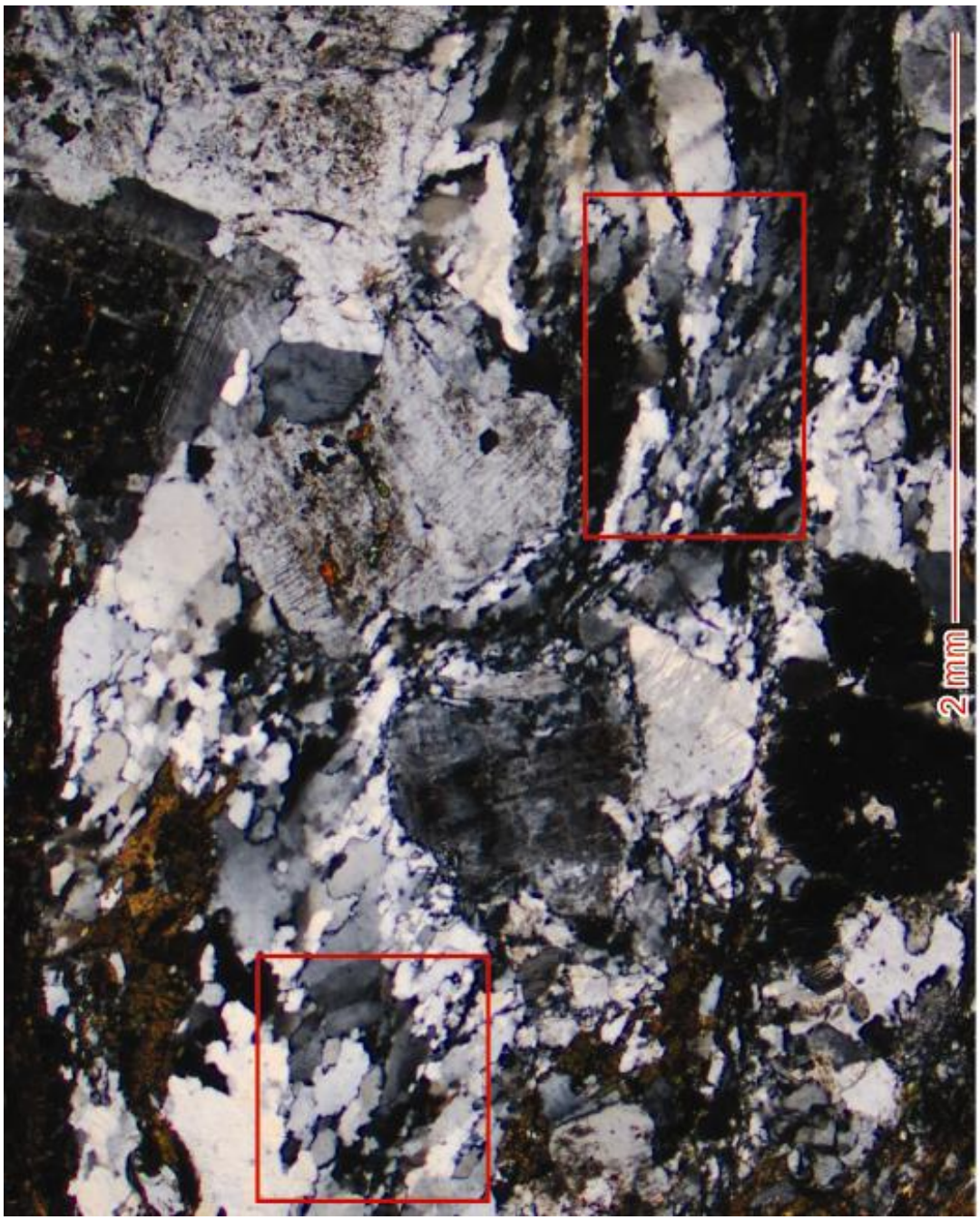

Figure 9

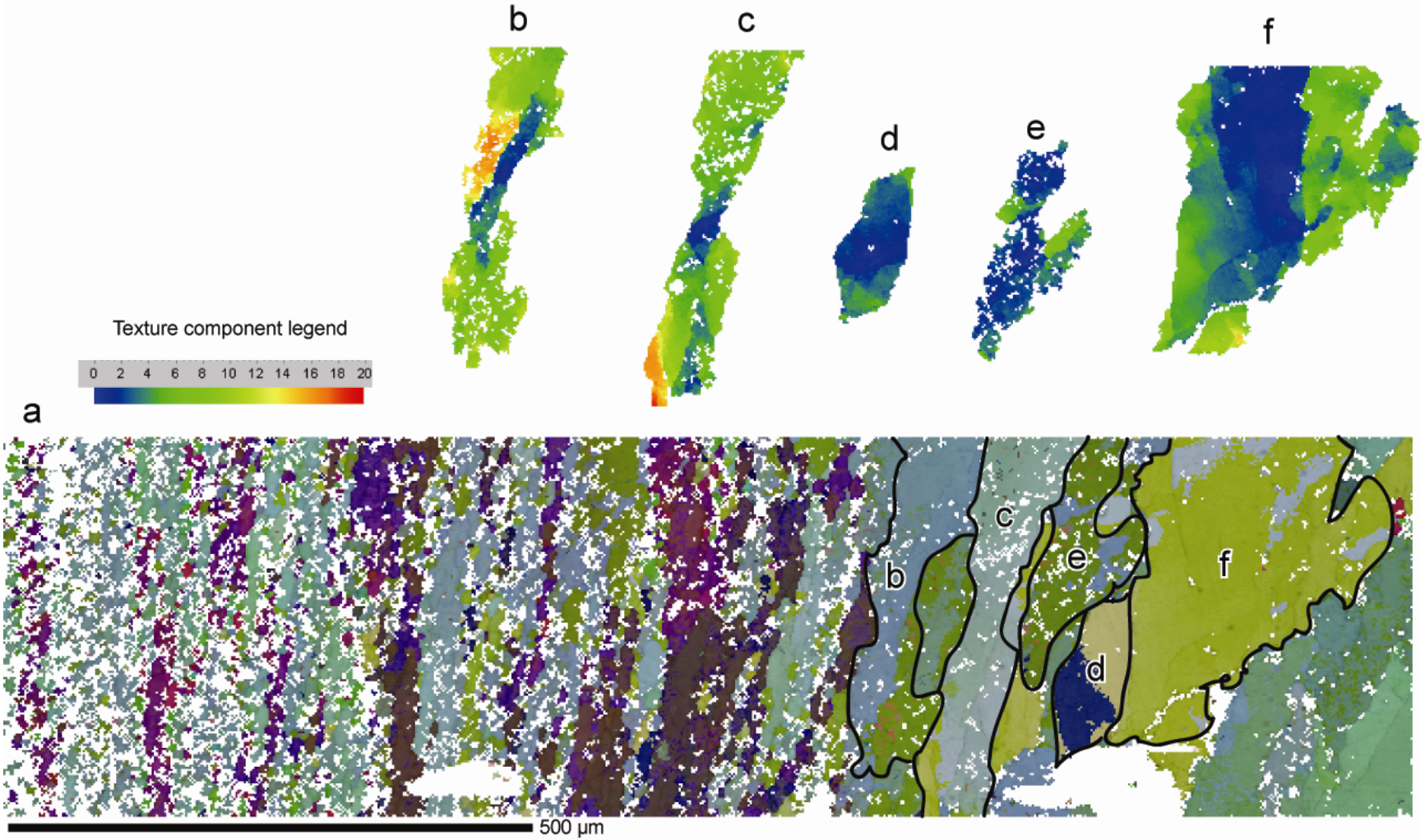
b
c
d
e
f
Texture component legend
0 2 4 6 8 10 12 14 16 18 20
a
b
c
d
e
f
500 µm

Figure 10

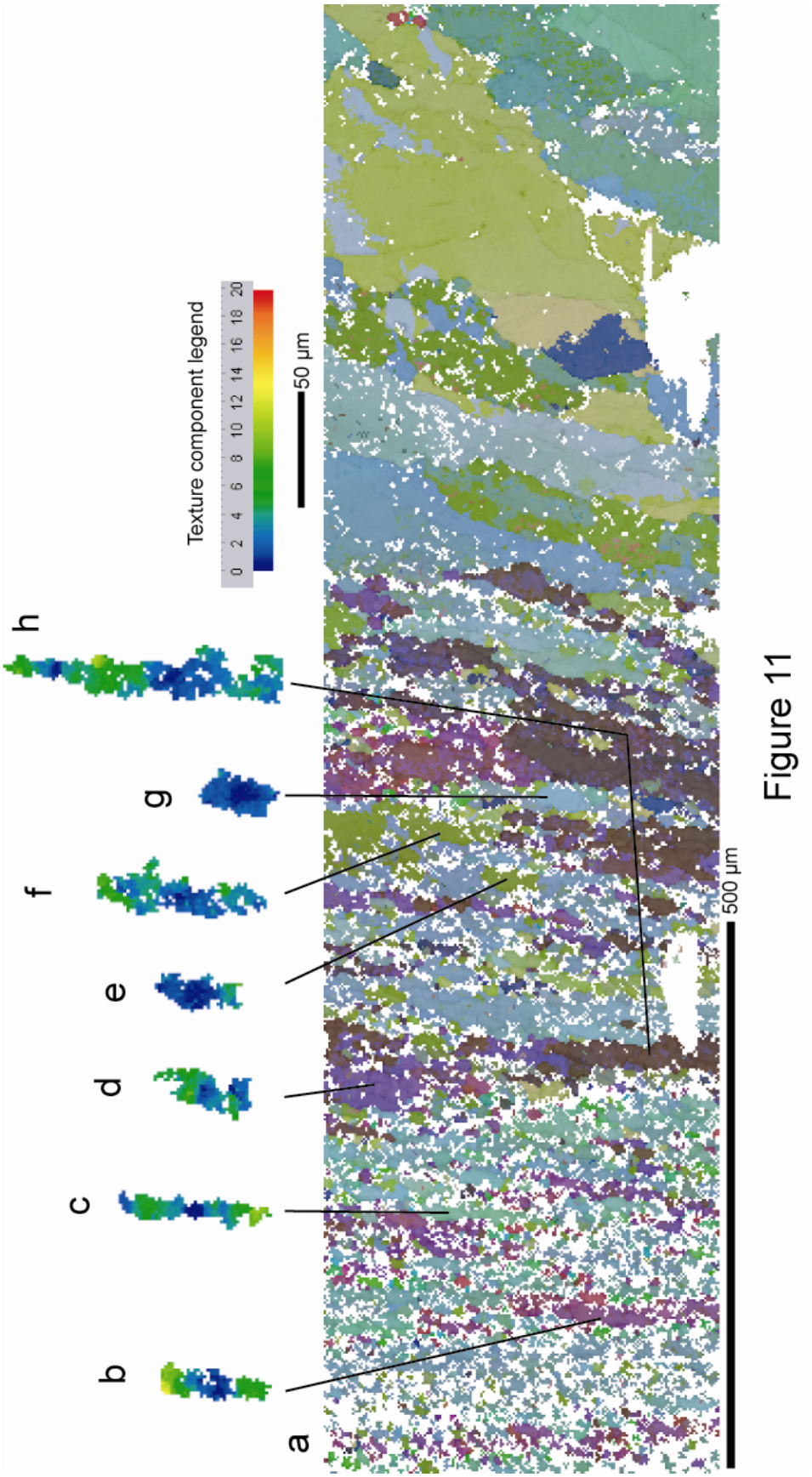
Texture component legend
0 2 4 6 8 10 12 14 16 18 20
50 µm
500 µm
a
b
c
d
e
f
g
h

Figure 11

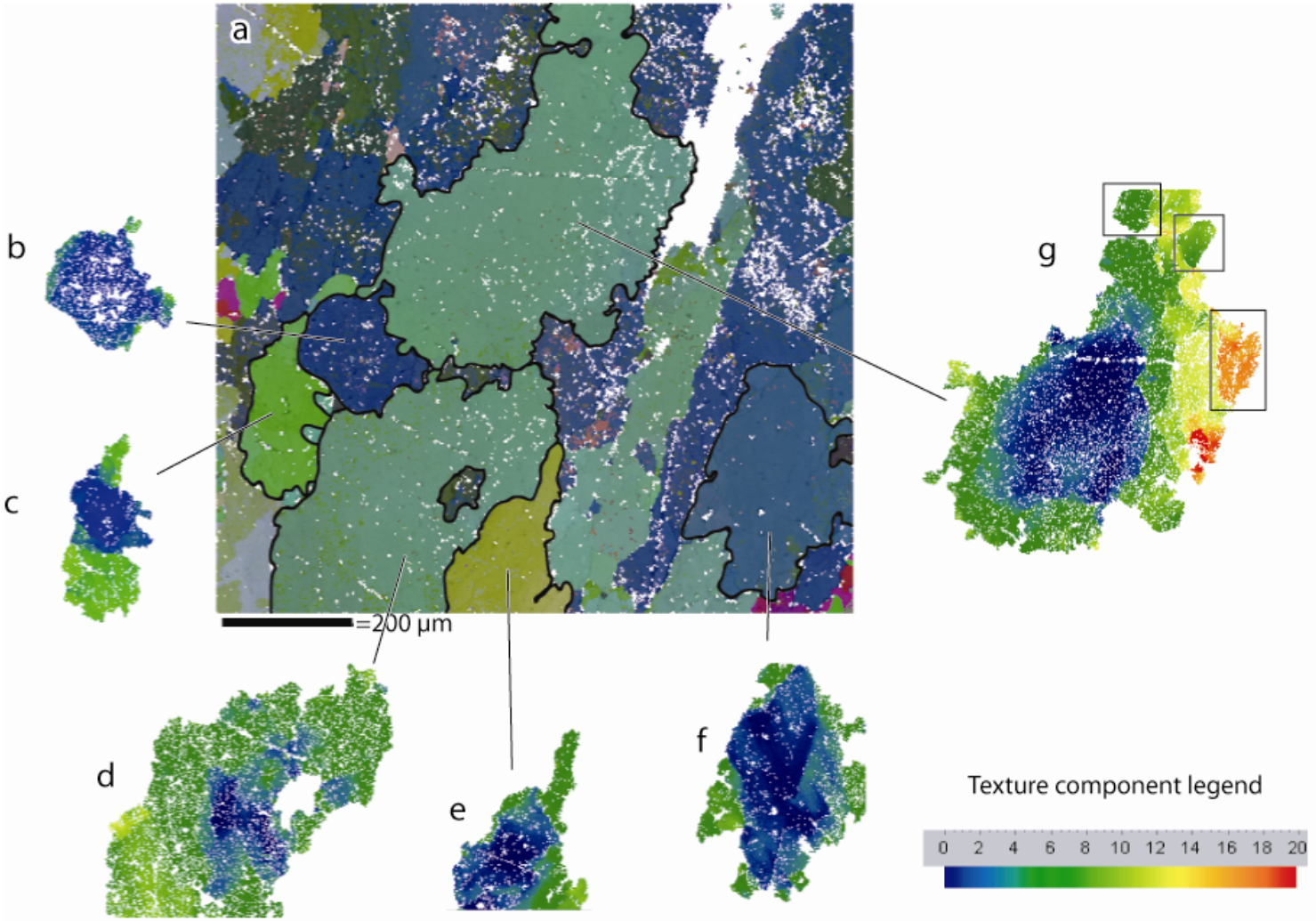
a
b
c
d
e
f
g
=200 µm
Texture component legend
0 2 4 6 8 10 12 14 16 18 20

Figure 12

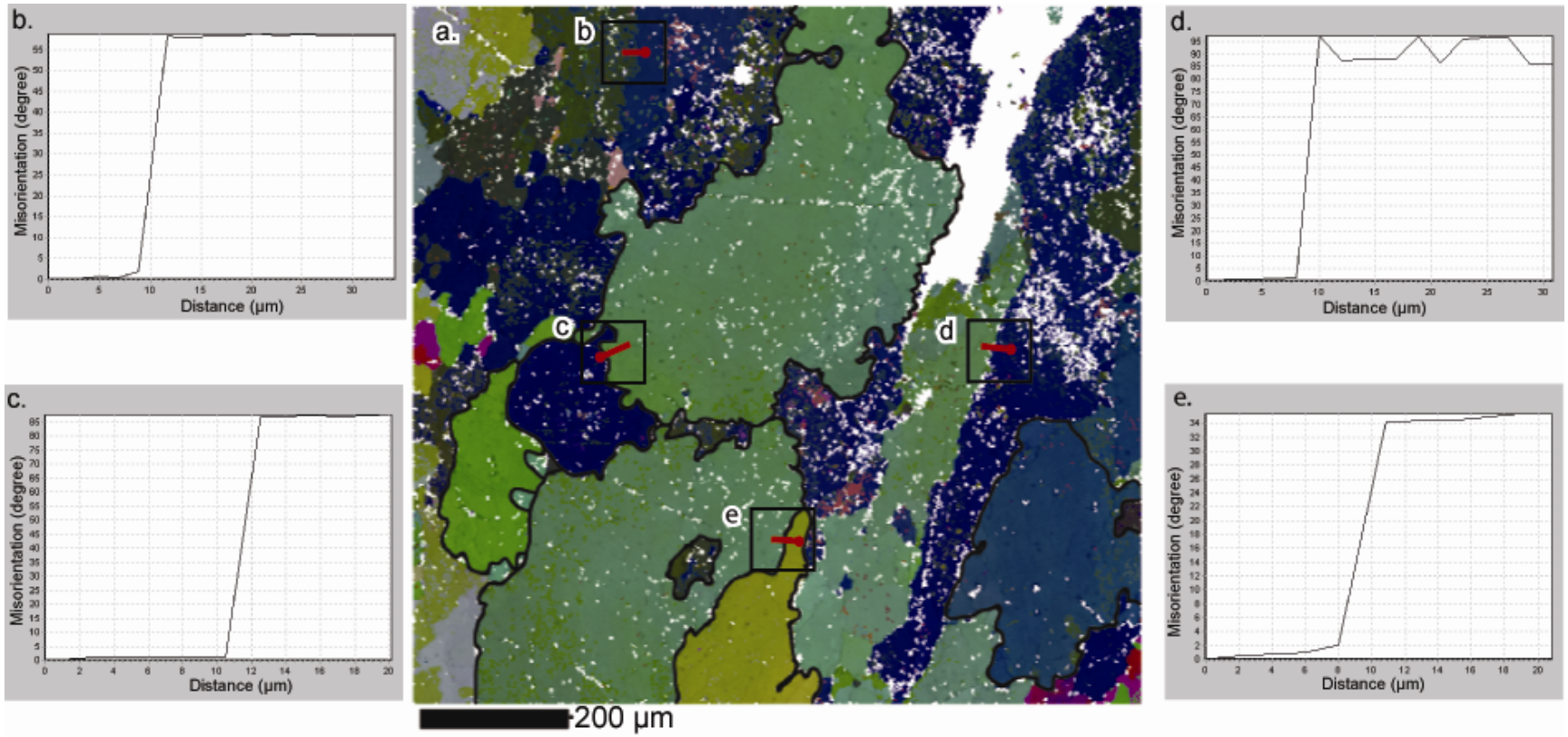

Figure 13

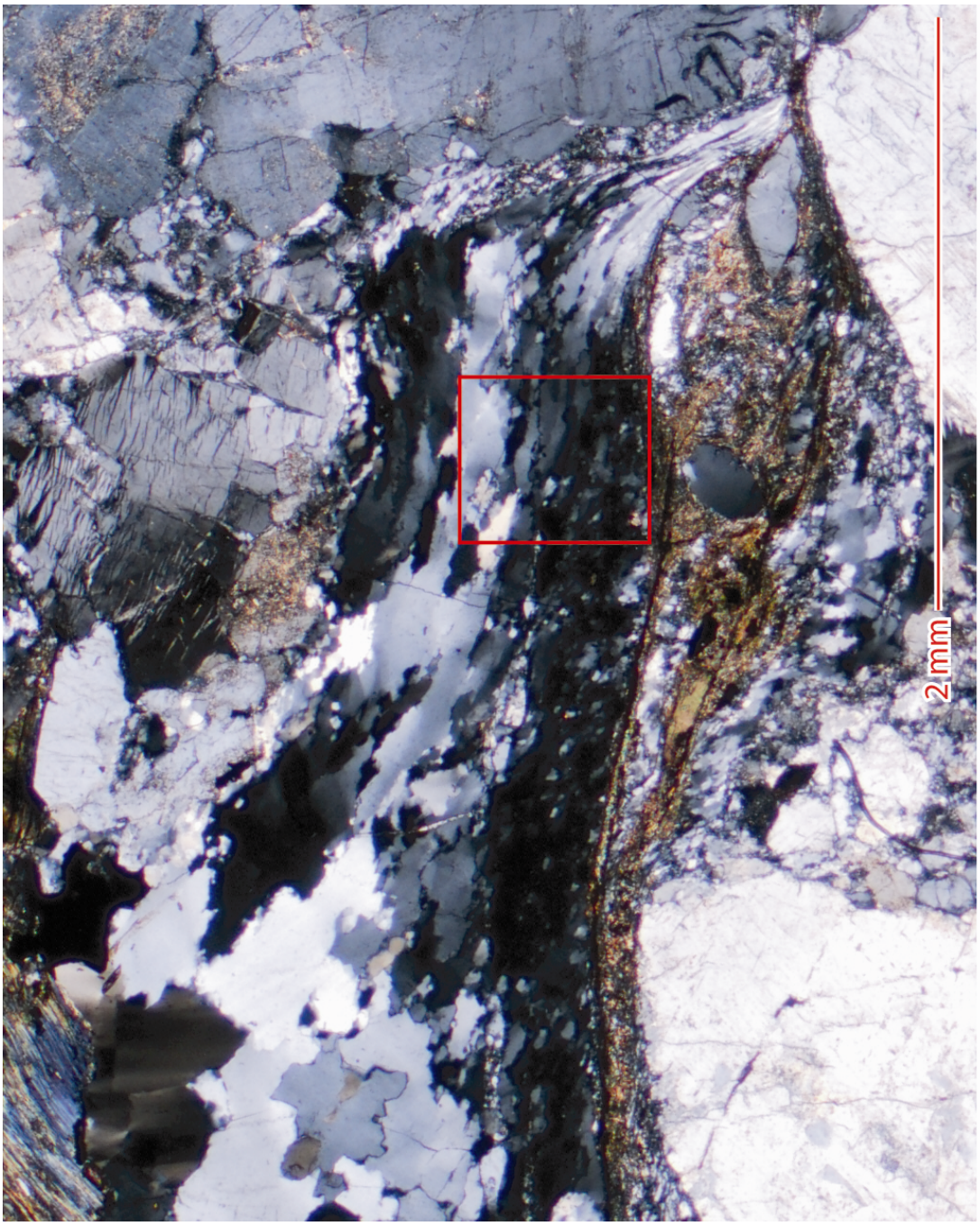

Figure 14

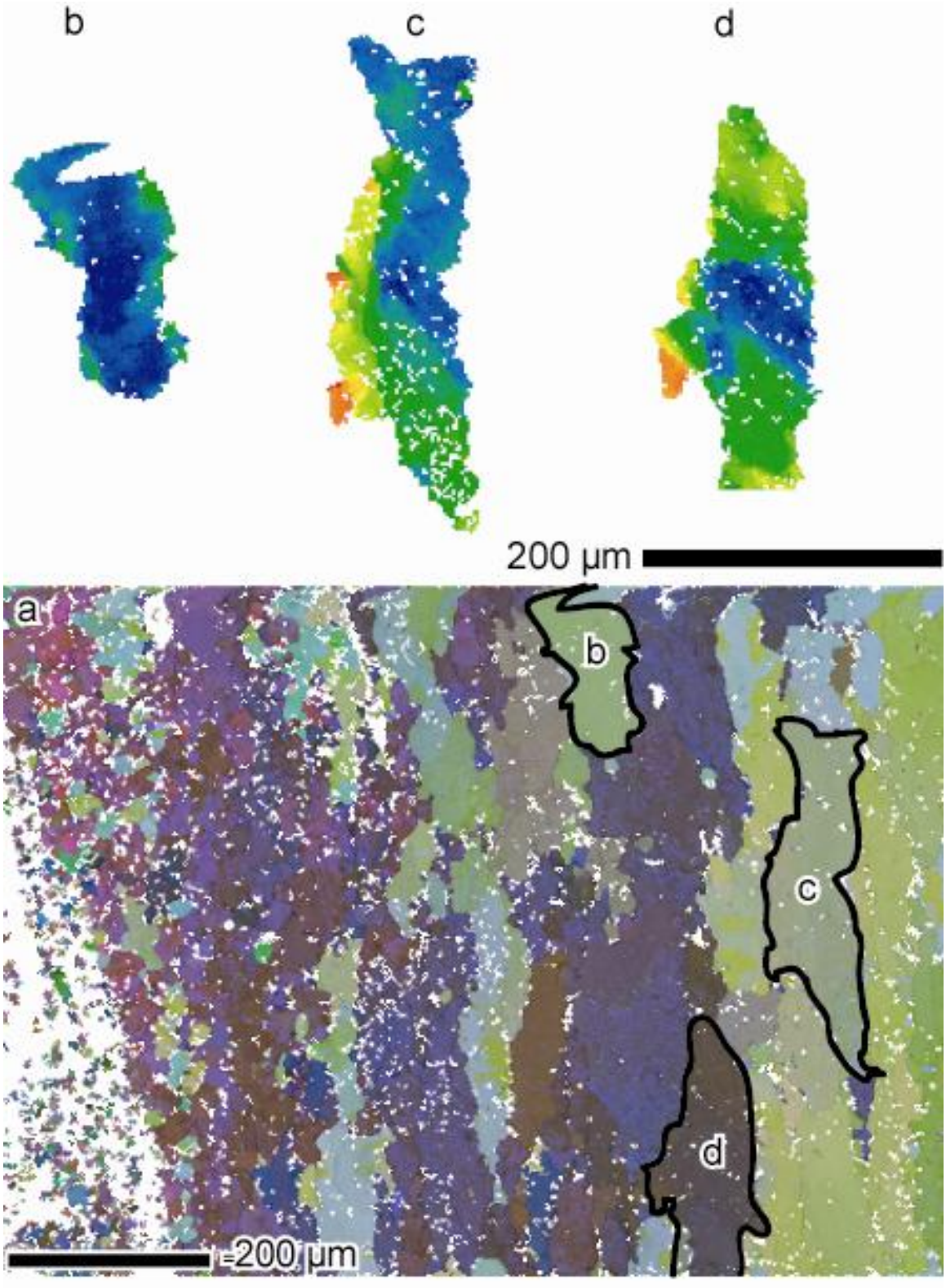

Figure 15

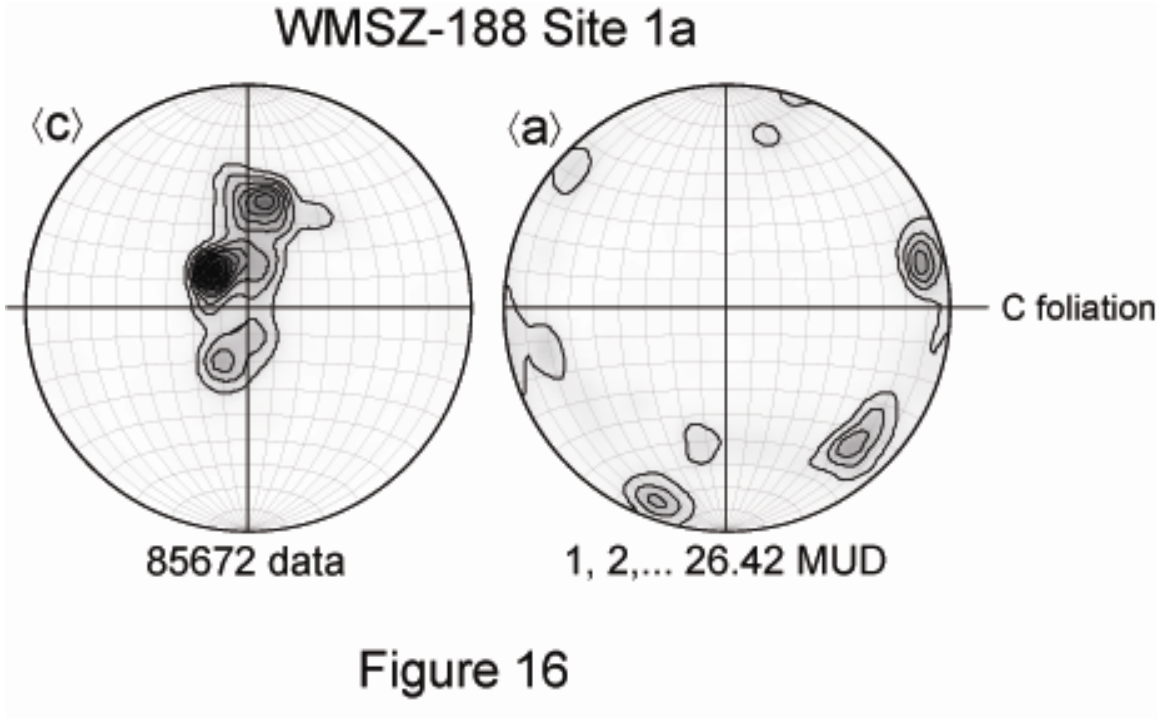

Figure 16

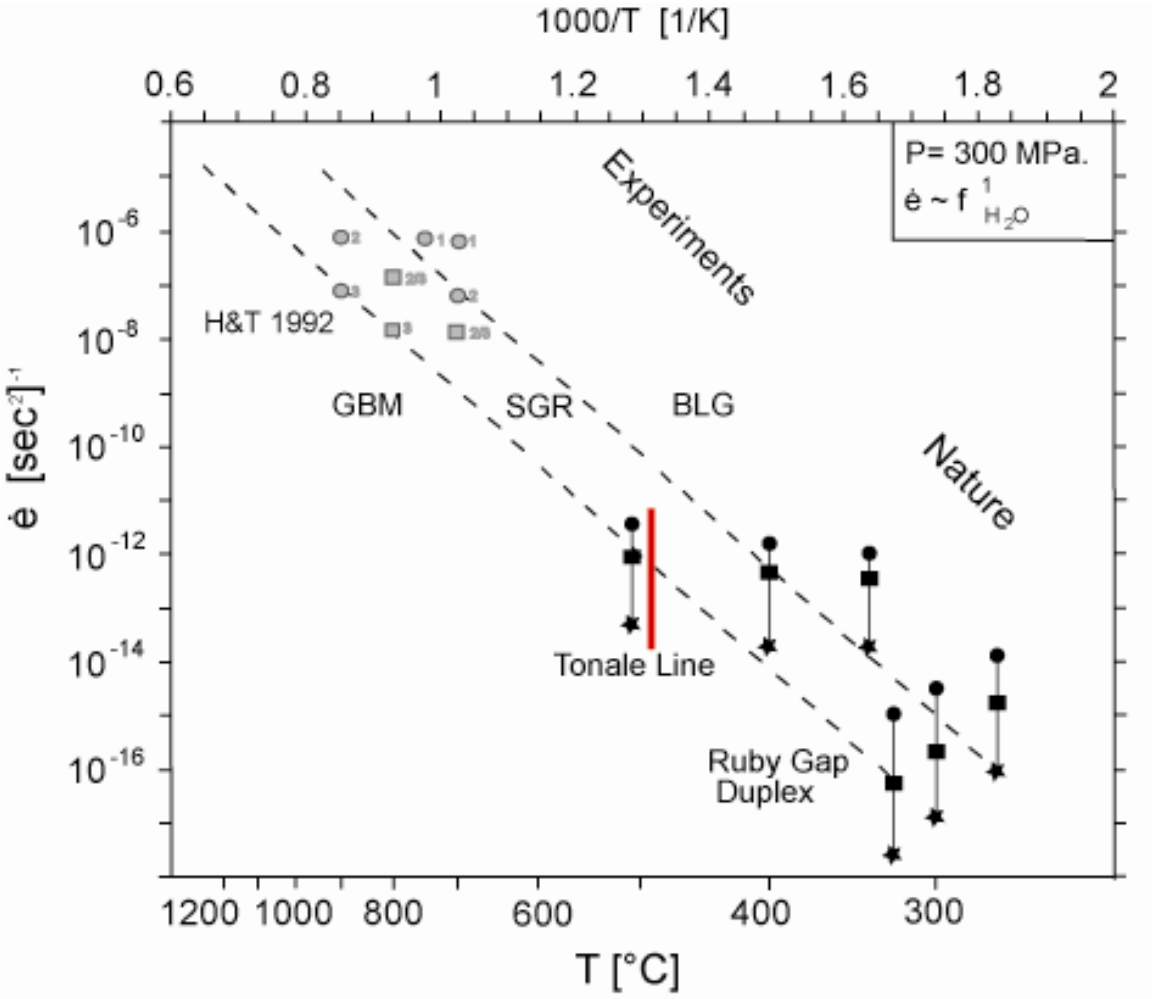
1000/T [1/K]
0.6
0.8
1
1.2
1.4
1.6
1.8
2
P= 300 MPa.
ė ~ f H2O 1
Experiments
H&T 1992
GBM
SGR
BLG
Nature
Tonale Line
Ruby Gap
Duplex
ė [sec-1]
10-6
10-8
10-10
10-12
10-14
10-16
1200
1000
800
600
400
300
T [°C]

Figure 17

APPENDIX A.

Electron Backscatter Diffraction

Electron Backscatter Diffraction (EBSD) uses back-scattered electron patterns to identify minerals and their crystallographic orientations. A thin section of rock is placed into the chamber of a Scanning Electron Microscope (SEM). Once the chamber is at vacuum, a beam of accelerated electrons bombards the sample. The electrons interact with the atoms that make up the crystal structure of the minerals. The electrons then diffract out of the sample, some of which are detected by a phosphor screen that is attached to a digital camera. The camera captures the images that are produced by the back-scattered electrons. These patterns, or Electron Backscatter Patterns (EBSP), are comprised of dark and light grey bands, called Kikuchi bands. These bands illustrate the lattice planes off of which the electrons diffracted. Based on the mineral and its orientation, the Kikuchi bands will appear a certain way and will change as the orientation changes (different patterns).

The ideal EBSPs are stored in a database and are used to identify the minerals and their orientations. The stored EBSPs are in the form of outlined Kikuchi bands. During the indexing process, the software attempts to find the best fit of the simulated EBSPs over the acquired EBSP. Any degree of error is referred to as the mean angular deviation (MAD). The maximum MAD and band detection parameters can be specified so that any degree of misorientation over a certain limit are not indexed and are considered as a point of no solution.

HKL software is used to make maps of crystallographic orientation over a given area. After locating the area and focusing the image, one simply inputs the dimensions of map area, determines the step-size, or distance between each sampling point, then sets up a “run”. The stage automatically moves in a grid pattern according to the parameters that were set up until the entire area has been imaged and indexed.